Neuroscience Vol. 14, No. 1, pp. 111–131, 1985
Printed in Great Britain

0306-4522/85 $3.00 + 0.00
Pergamon Press Ltd

MEMBRANE RESISTIVITY ESTIMATED FOR THE PURKINJE NEURON BY MEANS OF A PASSIVE COMPUTER MODEL

D. P. SHELTON
Department of Physics, University of Toronto, Toronto, Ontario, Canada M5S 1A7

Abstract—A multicompartment passive electrotonic computer model is constructed for the cerebellar Purkinje cell of the guinea-pig. The model has 1089 coupled compartments to accurately represent the morphology of the Purkinje cell. In order that the calculated behavior of the model fit the published electrophysiological observations of somatic and dendritic input conductance, the neural membrane resistivity must be spatially non-uniform. The passive electrical parameter values for which the model best fits the observations of input conductances, pulse attenuation and current-clamp voltage transients are $r_{m,dend} = 45{,}740\ \Omega cm^2$, $r_{m,soma} = 760\ \Omega cm^2$, $r_i = 225\ \Omega cm$ and $c_m = 1.16\ \mu F/cm^2$ (the membrane and cytoplasm specific resistivities and membrane specific capacitance, respectively). The model with these parameter values is electrically compact, with electrotonic length $X = 0.33$ and dendritic dominance ratio $\rho = 0.44$.

Analysis of the calculated voltage transient of the multicompartment model by the methods of equivalent-cylinder cable theory is shown to result in very different and unreliable conclusions. The signficance for neuronal function of the estimated electrical parameter values is discussed. The possible effect of active conductances on these conclusions is assessed.

The transmembrane leakage conductance of a neuron plays an important role in determining the extent of the passive spread of synaptic potentials and therefore bears on the question of what sort of integration is performed by the dendritic tree of a neuron.[32,41,42,45,51] Estimates of the membrane leakage resistivity, r_m, for a variety of neurons have been made using both an equivalent-cylinder analysis[40,43,98] and multicompartmental models.[4,31,95] Often the analysis assumes a morphologically simplified model of the cell and uses "effective" parameter values which cannot be given a straightforward physical interpretation. We wish to construct a computer model of a neuron which is accurate in terms of morphology and electrical properties, and whose behavior is consistent with electrophysiological observations. The immediate objective is to estimate the passive properties of the neuron being modelled. This passive neuron model would form the substrate for extensions which would treat more complex properties.

We choose to model the Purkinje neuron for several reasons. Firstly, both the morphology[6–12,25,26,55,85] and electrophysiology[26,54–58,85,90] of the cerebellum and the Purkinje cell have been extensively and intensively studied. This provides a wide base of information to draw on. Secondly, we require detailed and complete information on the anatomy of the particular neuron being modelled. The form of the Purkinje cell dendritic tree, a flat fan, is ideal for mapping out the entire dendritic tree of a particular cell. Thirdly, the organization of the cerebellar cortex is relatively simple and constant, both over the extent of the cortex in any one animal and also between different species. This uniformity facilitates synthesis of the results obtained in different preparations. Also, since the sole output channel for the Purkinje cell is its axon (and perhaps its extracellular microenvironment[64]), one may simply interpret function in terms of effect seen at the soma, without the added complication of local circuits.[82] Finally, the part of the dendritic tree of the Purkinje cell which is thought to be essentially passive forms a very large fraction of the total membrane surface area of the cell. This will tend to make estimates of the passive membrane properties more reliable.

One must note however, that the presence of various active conductances, which manifest themselves for even small depolarizations from rest,[3,20,57,58,61,83] requires that the suitability of a passive model be regarded as an assumption rather than a foregone conclusion. This *caveat* applies to all neurons, but is most difficult to dismiss in the case of a neuron with a complicated dendritic tree which may be partly active.

EXPERIMENTAL PROCEDURES

In order to accurately estimate the membrane resistivity for a neuron, one must meet several requirements. Firstly, one must have a model which faithfully represents the electrotonic structure of the neuron. Secondly, one must be able to specify all the morphological parameters required by the model. Thirdly, one must be able to fix, or at least constrain, the values of the electrical parameters which enter the model, such that only the membrane resistivity is a free parameter. Lastly, one requires suitable experimental measurements to which to fit the model. We consider each of these points in turn.

Compartmental model and computational method

We have used a compartmental model[31,45,51,56,68,69,92-94] for the Purkinje neuron since this type of model is the most flexible and has the fewest built-in assumptions. The basic assumptions are, that the dendrites are a system of connected membrane cylinders in which the intracellular current flow is essentially parallel to the cylinder axis of each compartment, and that the resistance of the extracellular circuit is negligible. The first assumption is valid when the transmembrane impedance is very large compared to the resistivity of the cytoplasm. The second assumption requires that the resistivity of the extracellular medium be comparable to or less than the resistivity of the cytoplasm, and that the volume for current flow in the extracellular loop be much less restricted than in the intracellular circuit. Even during synchronous activation of cortical neurons, the extracellular potential gradients are much smaller than the intracellular gradients.[54] When a small current is injected into a single neuron, as is the case in this study, then a very large extracellular volume will effectively contribute to the extracellular loop and the potential gradients are expected to be entirely negligible.[38,41,72]

The branching of the Purkinje cell dendrites is incorporated into the compartmental model in a very direct fashion. The dendritic tree is dissected into simple, unbranched cylinders by cutting it at all its branch points. The compartments of the model are taken to be the dendritic segments extending between branch points. For each compartment of the model, we specify the length, diameter and connections with the rest of the network. The average length of the compartments in our model is about 12 μm and the average electrotonic length of the compartments, for $r_m = 10^4\ \Omega\text{cm}^2$ and $r_i = 100\ \Omega\text{cm}$, is about 0.02. Thus, dissection of the dendritic tree at the branch points yields compartments which are electrotonically very short. Since the compartments are short, we may represent each compartment to sufficient accuracy with lumped resistors and capacitors[56,68,69] rather than using the finite cable equations.[31,45,72-75,77,95]

The complete specification of a compartment in terms of lumped electrical elements is comprised by the axial resistance of the cytoplasm in the cylindrical compartment, R, the total transmembrane conductance of the compartment, G, the equilibrium potential of the transmembrane conductance, V_Q, and the total membrane capacitance of the compartment, C. For a smooth, right-circular cylindrical compartment with passive membrane, one has:

$$R = 4Lr_i/\pi D^2,$$

$$G = \pi LD/r_m,$$

$$C = \pi LDc_m,$$

where r_i is the cytoplasm resistivity, r_m is the membrane passive leakage resistivity, c_m is the membrane specific capacitance, L is the cylinder length and D is the cylinder diameter. In the case of the spiny dendrites, the surface area of the compartment is increased from πDL to $\pi DL + N_{sp}A_{sp}L$, where N_{sp} is the linear density of spines and A_{sp} is the surface area of a spine. The expressions for G and C are modified accordingly. In addition to the membrane leakage contribution to G for the compartment, one may include parallel conductances due to synaptic activation, voltage-sensitive channels or a current-injecting microelectrode. The total conductance G is then the sum of all the individual contributions:

$$G = \left[\sum_i G_i\right],$$

and the resultant equilibrium voltage for the total conductance G is:

$$V_Q = \left[\sum_i V_{Qi}G_i\right] \Big/ G.$$

In the present model, the only contributions to G come from the membrane leakage and the recording microelectrode.

Once the electrical parameters and connectivity of each compartment have been specified, two calculations may be carried out. The first calculation determines the output conductance of the model neuron, measured at a specified position on the soma or dendrites. The second calculation finds the voltage transient in response to switching on a constant current which is injected into the model neuron at a specified location. The compartmental model and the computational method are illustrated in Fig. 1.

The output conductance calculation uses the recursive procedures shown in Fig. 1(C), (D), starting at the dendritic terminal segments and moving inwards to the chosen output node.[4,72,95] The most general pattern of connectivity for a dichotomously branched network is shown in Fig. 1(B), where the orientation of each compartment is defined such that the segment output end is nearest to the chosen output node. All terminal segments are assumed to have sealed ends—the sealed ends have zero conductance and the axial current is zero at the terminus. The steady-state compartment voltages may be calculated by a similar recursive procedure, working from the output node up to the dendritic terminals instead. These calculations are computationally very fast.

The calculation of the network voltage time evolution is done by integrating the coupled differential equations of the sort shown in Fig. 1(E).[56,68,69,92] The initial voltages are obtained from a steady-state calculation. The stimulus is a constant current switched on at $t = 0$. Because of the manner in which the dendritic tree is dissected into compartments in our model, many of the segments are very short. Numerical stability with a direct integration method such as Euler's rule requires time steps ranging down to a few nanoseconds. This is unfavorably short compared to the time scale of a few milliseconds for the network voltage variations. An implicit integration method, the trapezoidal rule, is stable for all step sizes and so is more suitable for such "stiff" problems.[24,30] Integration was done by the trapezoidal method. The size of the time step used was varied according to the accuracy desired and was typically of order 10 μs. A single time step of the full model with 1089 compartments, described below, required about 1 s on a VAX 11/780 computer.

Morphology

The detailed anatomy of our model is based mainly on the dimensions and topology measured for a particular Golgi-stained Purkinje cell from an adult rat. Comparison of Golgi-stained and horseradish peroxidase-injected Purkinje cells indicates that the entire dendritic arbor is visualized in the Golgi preparation.[9,10,12,55] Because of the thin, flat, fan-shaped form of the dendritic tree, measured segment lengths and diameters will be substantially unaffected by foreshortening. The original drawing of our examplar cell is given in Fig. 6 of Ref. 6. This cell is depicted in Fig. 2, before and after pruning off the spiny branchlets. The connectivity and dimensions for all the dendritic segments of this neuron are shown in Figs 3 and 4. The model neuron exhibits purely dichotomous branching, in agreement with observations.[6,7] In any case, the computational model is insensitive to the topological distinction between several closely spaced bifurcations and a single node of higher branching order. Two questions must be borne in mind when evaluating the morphological adequacy of our model. The first question is whether this single cell is an adequate exemplar. The second question is whether the morphological parameters of the given cell can be sufficiently accurately determined. We will defer discussion of these questions until later.

While we have detailed anatomical information for the rat Purkinje cell, the most detailed electrophysiological measurements have been made on the larger guinea-pig Purkinje cell.[57,58] One may ask whether it is possible to use

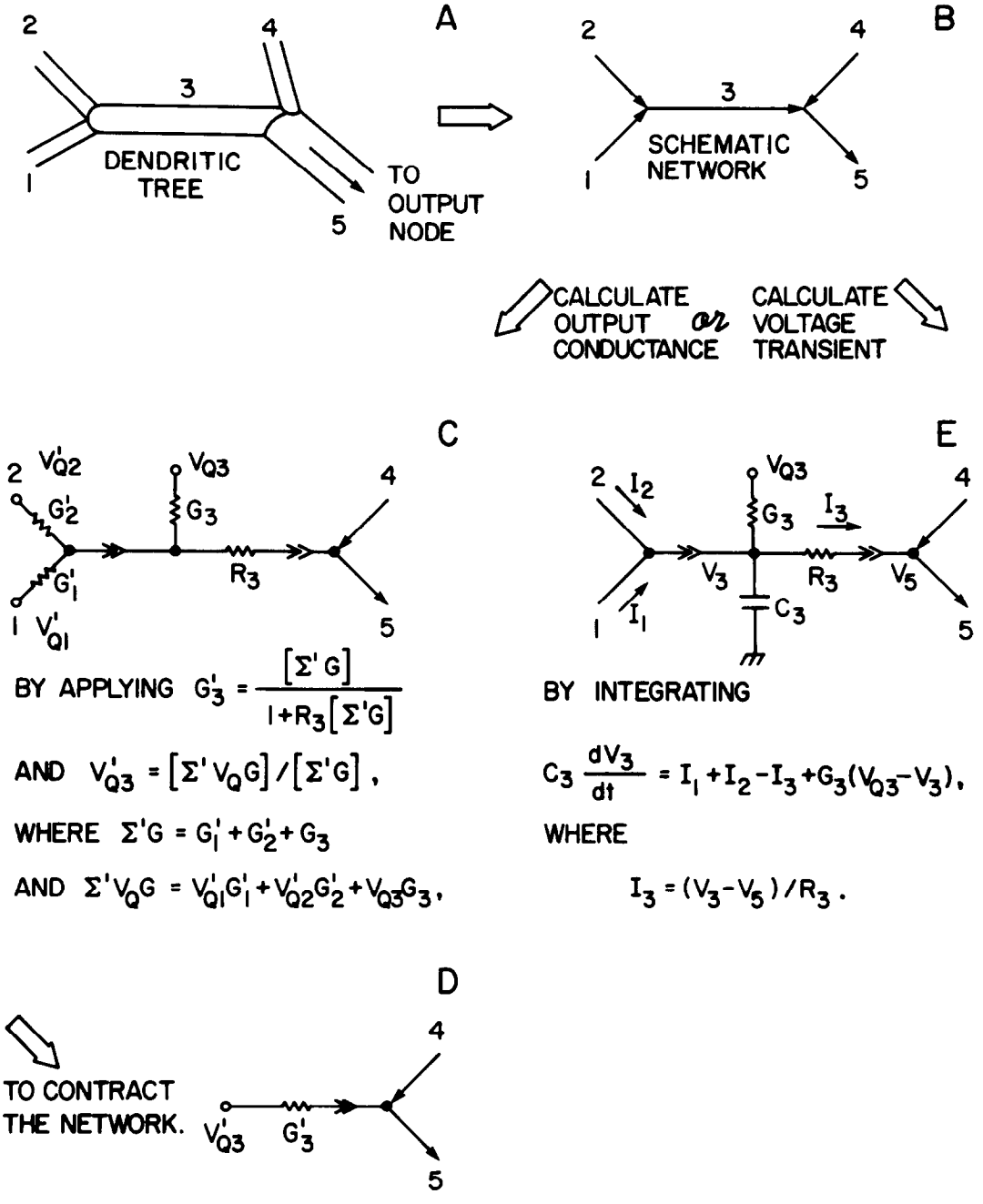

Fig. 1. Compartmental model and computational method. (A), (B) The membrane cylinders composing the dendritic tree are dissected at branch points to give the compartments of the network representing the neuron. (C), (D) In the steady-state analysis, successive applications of the recursive procedure shown contracts the network until it is represented by a single conductance. (E) In the dynamic simulation, each time step involves integrating the differential equation shown, for every compartment in turn.

the anatomical information pertaining to the rat Purkinje cell to describe the guinea-pig Purkinje cell as well. Comparing Plate 1 of Ref. 57 and Fig. 4 of Ref. 58 with our Fig. 2, one sees that the rat and guinea-pig Purkinje cells are qualitatively similar in appearance. Furthermore, the count of 73 spiny networks feeding the smooth dendritic tree shown in Fig. 4 of Ref. 58 for the guinea-pig is in close agreement with the value of 86 for the number of spiny networks for the rat cell shown in Fig. 2, especially when allowance is made for ambiguity in partitioning the spiny networks. The pattern and complexity of dendritic branching appears to be similar for Purkinje cells of the two species.

One may compare the relative size of the Purkinje cells of the two species on the basis of four measures: (1) the depth of the molecular layer, (2) the soma diameter, (3) the diameter of the largest dendritic branch point and (4) the maximum dendritic length from the soma to a dendritic terminal. For our rat Purkinje cell the values of these four dimensions are 240, 22, 8 and 236 μm, respectively. The depth of the molecular layer in the guinea-pig is 300 μm.[39] Using this depth to set the scale of Fig. 4 of Ref. 58, we

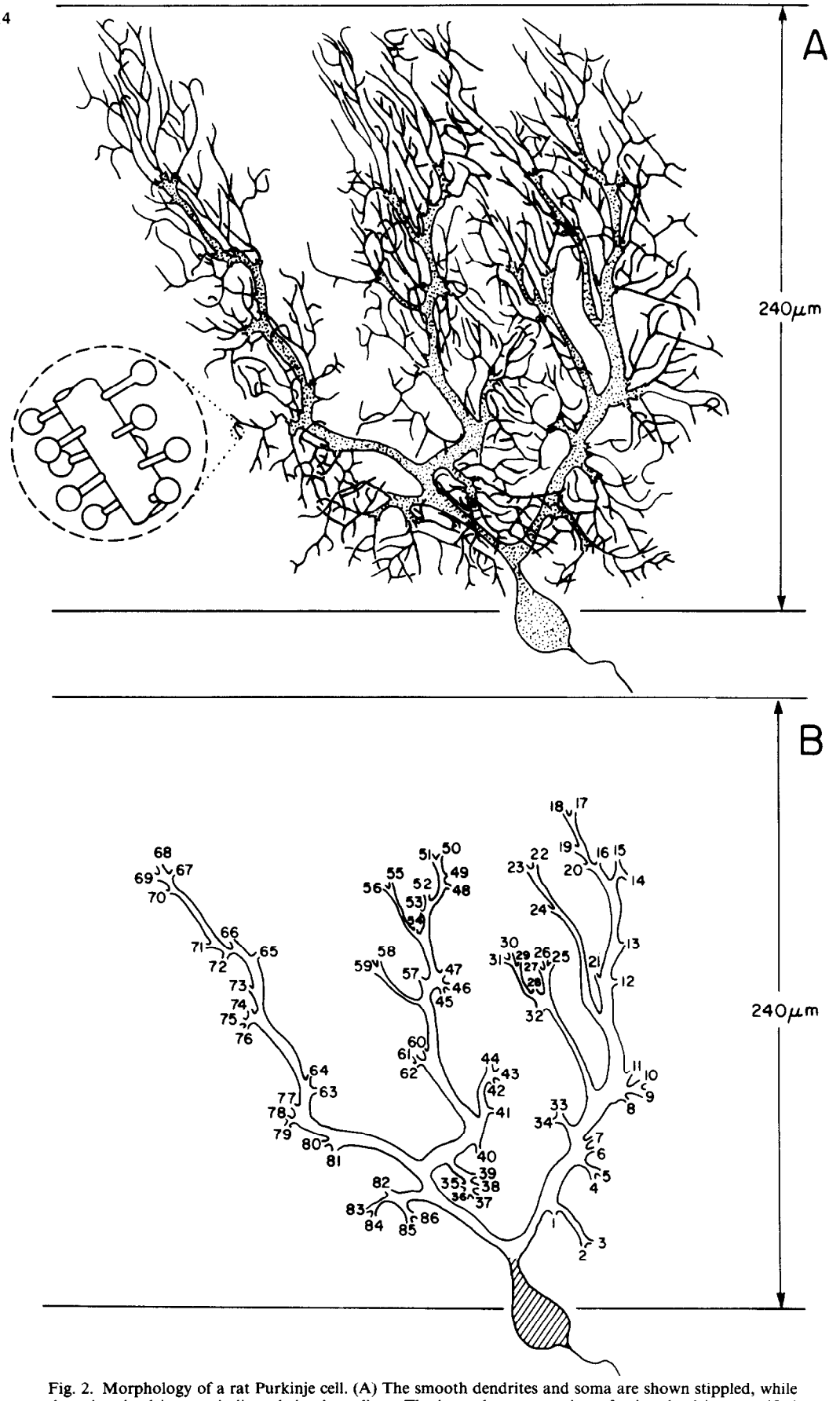

Fig. 2. Morphology of a rat Purkinje cell. (A) The smooth dendrites and soma are shown stippled, while the spiny dendrites are indicated simply as lines. The inset shows a portion of spiny dendrite magnified 20 ×. The top and bottom boundaries of the molecular layer are indicated by the horizontal lines. (B) All branches of Strahler order 3 or less have been removed to reveal the smooth dendritic tree. The labels for the points of attachment of the amputated spiny networks are ordered counterclockwise around the dendritic perimeter. The region taken to be the soma is shown hatched.

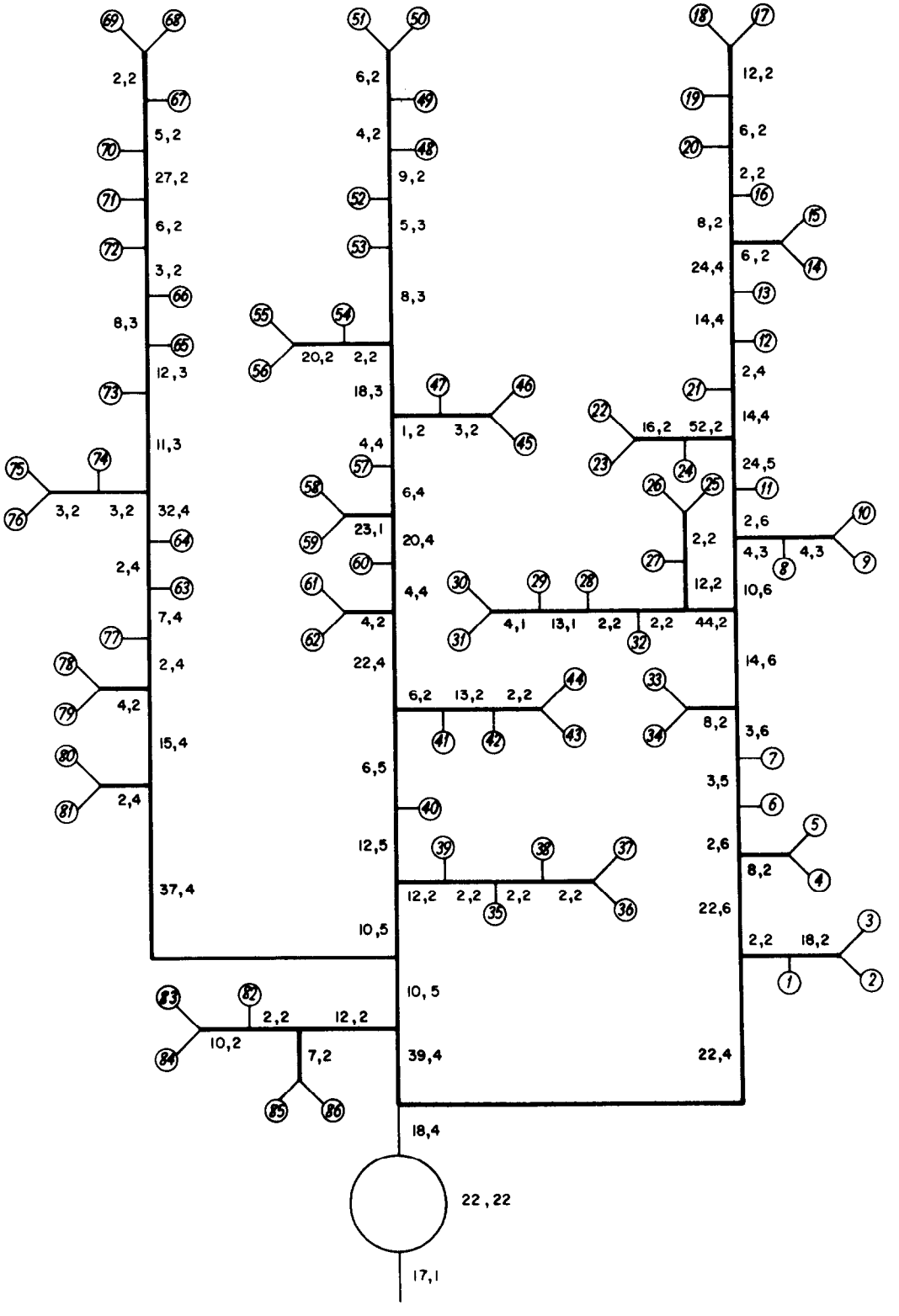

Fig. 3. Network representing the smooth dendritic tree of the rat Purkinje cell depicted in Fig. 2. The length and diameter (L, D in units of μm) of each compartment is as shown. The smooth dendritic segments are drawn as heavier lines and the attachment points for the spiny networks are marked by circled numbers. The guinea-pig Purkinje cell model uses the same smooth network with the dimensions of its compartments multiplied by a scale factor of 1.36.

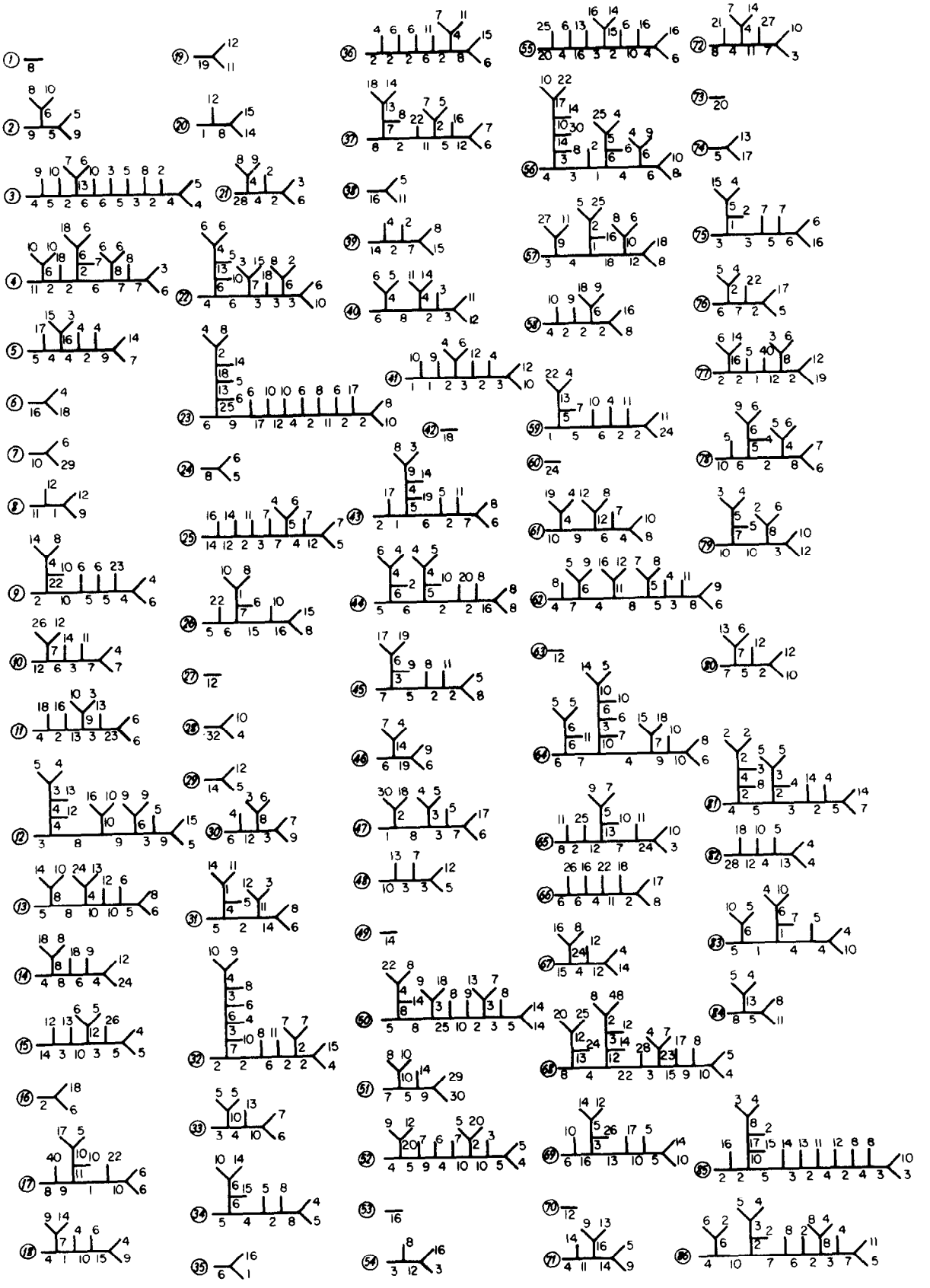

Fig. 4. Spiny dendritic networks for the rat Purkinje cell depicted in Fig. 2. The length (L in units of μm) of each compartment is as shown. The circled numbers which label the spiny networks correspond to the labels in Figs 2 and 3. The guinea-pig Purkinje cell model uses the same spiny networks with the lengths of their compartments multiplied by a scale factor of 1.36.

Table 1. Summary of the morphology of the guinea-pig Purkinje cell compartmental model

Strahler order	Number of segments	Total segment length (μm)	Average segment diameter (μm)	Segment description
1	544	7367	1.00	Spiny dendrites*
2	314	2981	1.40	Spiny dendrites*
3	144	1208	2.00	Spiny dendrites*
4	52	558	2.76	Smooth dendrites
5	24	466	5.22	Smooth dendrites
6	8	156	6.57	Smooth dendrites
7	3	78	13.67	Soma and initial axon segment

*4.4 spines/μm.

find the values for the other three parameters for the guinea-pig to be: soma diameter 34 μm, maximum dendritic branch point diameter 11 μm and maximum dendritic path length 300 μm. The ratios of these four measures for the two species (ratios 1.25, 1.55, 1.38, 1.27; average ratio 1.36 ± 0.14) are sufficiently consistent that, as a first approximation, one may take the guinea-pig Purkinje cell to be just a scaled up version of the rat Purkinje cell. Our model of the guinea-pig Purkinje cell uses the dendritic networks shown in Figs 3 and 4, but applies a multiplicative scale factor of 1.36 to all the dimensions shown in those figures. The lengths and diameters given in Figs 3 and 4 for the dendritic segments were measured directly from the drawing of the Golgi-stained rat neuron[6] while the dimensions of the axon initial segment were obtained from the results of a serial electron micrographic reconstruction.[86] Note that histological shrinkage of the smooth dendrites and soma is accounted for since the scale of the model is set using the depth of the molecular layer measured in living tissue.[39]

The dendritic tree of our model has been partitioned into spiny branches of Strahler order 1, 2 and 3 with the remainder of the dendritic tree being composed of smooth branches. In support of this assignment we call upon several lines of evidence. Micrographs show an abrupt transition between smooth and spiny branches[2,12] and it has been noted that the transition from spiny to smooth dendrites occurs at branches of the fourth Strahler order.[37] Electron micrographic spine counts vs branch diameter are consistent with transition at this order of branching.[50] The appearance of the dendritic tree after trimming off the first, second and third order branches agrees with the appearance of the smooth dendrites in degree of branching and spatial extent.[37] The climbing fiber, which contacts the smooth dendrites exclusively, also shows branching patterns which match our pruned dendritic tree.[12,37,55,56] Finally, since most of the total dendritic length falls on branches of the first and second Strahler order (Table 1), the estimate of the total number of dendritic spines is fairly insensitive to the exact choice of the spiny-to-smooth boundary position.

It is found that the diameters of the terminal dendritic segments are tightly clustered around 1.0 μm, and that the segments of the distal dendritic tree are untapered and have a branching power of 2.0.[36] This implies that the cross-sectional area of the dendritic segments is conserved at each branch point. Since we know the number of spiny branches of each order for our model (Table 1), we may use the conservation of cross-sectional area and the average terminal branch diameter to deduce the average dendritic diameters for the spiny branches of each order. We obtain 1.0, 1.4 and 2.0 μm as the dendritic diameters of the first, second and third order segments.

In addition to the length and diameter of each spiny branch, one must specify the number and form of the spines which are attached to its surface. The measured linear density of spines is constant at 4.4 spines/μm for mouse,[50] cat[26] and man.[26] Only when one considers the primitive cerebellum of the frog does the spine density fall to a significantly lower value (1.1 spines/μm).[87] Accordingly, we have assumed that the spiny dendrites of our model are uniformly covered with 4.4 spines/μm of dendritic length. The form of the spines is taken to be that of a spherical head 0.5 μm in diameter attached to the dendrite by a cylindrical stalk 0.7 μm long and 0.14 μm in diameter.[48,55] Each spine adds 1.1 μm^2 to the total surface area of the dendritic segment on which it resides. The spiny branch diameters, spine density and spine dimensions are assumed to be the same for both rat and guinea-pig Purkinje cells. While it is difficult to quantitatively assess such factors as shrinkage because of the diverse sources for the above data, the self-consistency of the final model indicates that no gross errors have been incurred. Our guinea-pig Purkinje cell model is invested with 50,846 spines, within the range of experimental estimates for the total number of spines per Purkinje cell.[26,55,67] The surface area of the spines alone comprises nearly half the total cell membrane surface area of 118846 μm^2, while the spiny dendrites altogether comprise 84% of the total area. The smooth dendrites and soma comprise 13.2 and 2.8%, respectively.

Electrical parameters and electrophysiological observations

Membrane capacitance. The passive model of a neuron is characterized by the specific capcitance, resistivity and resting potential of the cell membrane and by the resistivity of the cytoplasm. The first of these parameters, the specific capacitance of the membrane, c_m, is of the nature of a biological constant. The value of c_m is set by the near constant thickness and dielectric constant of the hydrophobic core of the ubiquitous bilayer membrane (proteins make up about half the weight of biological membranes but have nearly the same polarizability as the lipids[70]). In all preparations where c_m has been accurately determined, the specific capacitance has been found to have a value near 1.0 $\mu F/cm^2$.[19,28,28a,31,33,81] Experimental estimates of c_m substantially greater than this value[4,89,95] are most likely the result of having underestimated the membrane surface area. We initially assume $c_m = 1.0\ \mu F/cm^2$ for our model guinea-pig Purkinje cell, giving a total cell capacitance of 1188 pF. In the final analysis c_m is allowed to vary to give the best fit to the data. In this case, a substantial deviation of the calculated value of c_m from 1.0 $\mu F/cm^2$ will invalidate the model.

Cytoplasm resistivity. The other electrical parameters are functions of internal and external electrolyte composition and membrane permeability. For the *in vitro* slice preparation the extracellular ionic composition is that of the bathing solution. In the experiments[57,58] with which we intend to compare our model, the principal ions in the bathing solution were Na^+ (150 mM), K^+ (6.2 mM), Cl^- (131 mM) and HCO_3^- (26 mM). From measurements on other neurons bathed in similar extracellular solutions,[29,35]

and assuming no electro-diffusive potential for Cl^- across the resting membrane,[84] we estimate the main intracellular ions to be Na^+ (30 mM), K^+ (130 mM), Cl^- (10 mM) and organic anions (150 mM). From the tabulated conductivities of electrolyte solutions[79] one may readily estimate the resistivity of the extracellular fluid to be 50 Ωcm (at 37°C). Similarly, one estimates the resistivity of the intracellular fluid to be 67 Ωcm (at 37°C), assuming that all the ions are free and that the mobility of the organic anions is about one-fifth as large as that of Cl^-. The resistivity of the intracellular electrolyte may be increased somewhat from this value by the presence of a large concentration of organic solutes and by binding of some of the intracellular organic anions.[16,17]

However, the resistivities of the extracellular and intracellular compartments are not solely determined by the electrolyte solutions filling those compartments. One must also account for the very complex geometrical structure of the compartments. The extracellular medium resembles the liquid portion of a foam with a characteristic thickness (the intercellular space) of about 0.02 μm, while the intracellular medium is filled with various organelles whose membranes are not electrically transparent. Measurements of the diffusion of ions which do not leave the extracellular space show that the combined effects of tortuosity and volume fraction hinder the diffusion of ions in the extracellular medium of the cerebellar cortex by a factor of 12.[38,66] If current were confined to the extracellular space, then the resistivity of the extracellular medium would also be increased by a factor of 12, from 50 to 600 Ωcm. Direct measurements of the resistivity of the molecular layer show that its resistivity is anisotropic but homogenous with an average value of about 400 Ωcm.[65,99] The anisotropy of the resistivity and its reduction from the value deduced from the diffusion experiments is due to current crossing into the intracellular compartment. The alignment of the core conductors (e.g. axons and dendrites) in preferred directions accounts for the anisotropy, while the larger volume fraction available for current flow reduces the observed resistivity.[65,76] As an added complication, the observed resistivity of the medium will depend on the length scale over which it is measured, both because of the non-zero scale for the structure of the medium[66] and because of a characteristic length scale for current crossing out of the extracellular space.[76] The tip of a fine microelectrode probes the extracellular resistivity on a length scale (about 0.5 μm for a 0.1 μm diameter tip[27]) intermediate between the size of the 0.02 μm intercellular space within which the diffusion cofficients approach their free solution values, and the diameter of about 6 μm over which the structure of the extracellular medium seems to be averaged out.[66] The resistivity as seen by this microelectrode will lie somewhere between the corresponding values of 50 and 600 Ωcm, near 250 Ωcm.

Similar considerations apply to the intracellular medium though direct measurements of its resistivity are more difficult to come by. Axoplasm appears to be less highly structured than cytoplasm,[16] and its measured resistivity for a number of vertebrate and invertebrate species ranges from 20 to 160 Ωcm (one to four times larger than the resistivity of the intracellular electrolyte solution).[16,19,31,81] The measured resistivities of somatic cytoplasm are even more variable, falling between 70 and 390 Ωcm (one to eight times larger than the resistivity of the intracellular electrolyte solution).[4,16,17,81] Therefore, only the lower bound $r_i \geq 67$ Ωcm is fairly certain *a priori* for the Purkinje cell. The value of $r_i = 100$ Ωcm has been assumed by other authors.[41,69,92] We also take 100 Ωcm as a starting point, bearing in mind that r_i may in fact fall in the range 67–540 Ωcm. We assume that r_i is constant over the neuron, though it is entirely possible that it has different values for the axon, soma and dendrites. Our model is mainly sensitive to the value of the cytoplasmic resistivity of the dendrites.

It is important to consider the systematic errors which may be introduced into intracellular measurements by the non-negligible and possibly variable resistance of the glass microelectrodes used to make the measurements. The resistance of a micropipette microelectrode is composed of intraelectrode and extraelectrode components in series.[27,80,81] The intraelectrode component is the parallel combination of the glass surface conductivity (important for diameters of 0.1 μm or less)[80] and the volume conductivity of the concentrated electrolyte filling solution (diluted at the tip by diffusion).[49,71,80,81] The extraelectrode component of the electrode resistance is due to the convergence resistance of the relatively high resistivity medium surrounding the microelectrode tip.[27,81] A microelectrode filled with 3 M potassium acetate, having tip taper angle 5° and resistance 70 MΩ (in Ringer's solution) will have an inside tip diameter of about 0.06 μm (outside tip diameter of about 0.10 μm).[13,18,71,81] An important feature of such a fine microelectrode in our context is that the electrode resistance is sensitive to the resistivity of the medium in which it is immersed (chiefly through the convergence resistance term; iontophoresis also alters the electrode resistance when current is passed[71]), so that the bridge circuit used to allow simultaneous current injection and voltage recording with a single microelectrode[81,89] cannot remain balanced both before and after impalement of a neuron unless $r_e = r_i$.[27] Conversely, if the microelectrode-bridge circuit remains near balance both intracellularly and extracellularly, as appears to be the case for the experiments which we will consider (see Figs 3 of Refs 57 and 58), then the difference $|r_e - r_i|$ must be small (in order that the change in electrode resistance upon impalement is small compared to the input resistance of the neuron being probed). For the 70 MΩ electrode considered above, increasing the resistivity of the bath by 100 Ωcm will increase the electrode resistance by about 5 MΩ. Therefore, the intra- and extracellular bridge balance observed for 15 MΩ Purkinje cells implies that the extracellular resistivity of the cortex and the cytoplasmic resistivity of the Purkinje cell differ by less than about 50 Ωcm. These considerations favor an estimate of r_i near 250 Ωcm. Calculations were done for a range of r_i values.

Resting potential, input conductance and impalement leak. The Goldman equation[47,83] gives the resting membrane potential as a function of the external and internal ionic composition and the relative permeability of the membrane for the two principal permeant ions, Na^+ and K^+. Measurements of the resting potential[1,20,21,83,89,98] for several representative neuron types are consistent with the permeability ratio $P_{Na^+}/P_{K^+} = 0.02$.[21,83] Assuming this permeability ratio, we calculate the resting potential for the Purkinje neurons in Llinás and Sugimori's experiments[57,58] to be −72 mV, hyperpolarized with respect to the measured values. However, there is reason to suspect that the resting potential of the cell is significantly perturbed by the measurement process, in particular by the transmembrane leakage conductance due to imperfect sealing or damage at the site of impalement by the measuring microelectrode.[41] Accordingly, we will explicitly include the microelectrode leak in our model, in order that we may directly compare our calculations with the experimental observations.

For data we may consult the several recent intracellular studies of the Purkinje cell.[22,23,39,54–58,60] The relevant electrophysiological observables for our purposes are the input conductance, G_{in}, and the resting potential, V_{rest}, measured for intrasomatic and intradendritic penetrations. The best experimental estimates of these quantities for the guinea-pig Purkinje cell are $G_{in,soma} = 69.2 \pm 5.1$ nS, $V_{rest,soma} = -66.7 \pm 0.8$ mV (Table 2, Ref. 57, $n = 10$), $G_{in,dend} = 50.9 \pm 6.2$ nS and $V_{rest,dend} = -59.0 \pm 1.5$ mV (Table 1, Ref. 58, $n = 5$). These measurements were obtained for the cerebellar slice preparation and so are uncontaminated by synaptic conductances. The inequality of the intrasomatic and intra-

dendritic input conductances ($G_{in,soma}/G_{in,dend} = 1.36 \pm 0.19$) and of the intrasomatic and intradendritic resting potentials ($V_{rest,dend} - V_{rest,soma} = 7.7 \pm 1.7$ mV) are both highly significant results (95 and 99% confidence levels, respectively, Student's t-test). But the tip diameter of the 70 MΩ microelectrodes used in the measurements is sufficiently small that there should be no significant systematic error introduced into the measurements by the difference in diameter of somatic and dendritic impalement sites.[27] And, since systematic errors in bridge balancing would result in uniform misestimates of all the input conductances, the conductance ratio would be substantially unaffected by small balancing errors. To account for the unequal measured resting potentials one is forced to make some assumptions about the size of the impalement leak.

The impalement leakage conductance will appear in parallel with the output conductance of the cell at the impalement site to give the experimentally measured input conductance. If the impalement leak is not ion selective (reversal potential of 0 mV) and the resting potential of the unperturbed cell is $V_{rest} = -72$ mV, then an impalement leak of $G_{leak,soma} = 5.1$ nS for somatic penetrations and $G_{leak,dend} = 8.6$ nS for dendritic penetrations will account for the observed resting potentials. In neurons penetrated by microelectrodes of similar tip resistance (tip diameter) the impalement leakage conductance was found to be 5.2 nS,[1] in close agreement with our estimate for $G_{leak,soma}$. The larger value estimated for $G_{leak,dend}$ is consistent with the greater difficulty in obtaining satisfactory penetrations at dendritic impalement sites.[57] Blind penetration of the dendrites, giving deeper impalement and resulting in a larger hole in the cell membrane because of the substantial microelectrode tip taper, may account for the larger leak. Therefore, in our model we assume that the passive membrane resting potential is −72 mV, and that the neuron has been impaled by an imperfectly sealing microelectrode with $G_{leak} = 5.1$ or 8.6 nS depending on whether the impalement site is somatic or dendritic.

Membrane resistivity and further electrophysiological observations. At this point we note that all the passive electrical parameters of the model neuron have been specified, with the exception of the membrane resistivity r_m. All that is left to be done is to vary r_m for the model neuron until the calculated input conductance agrees with the experimental values given above. The model allows one to separately set the membrane resistivity for each of the anatomically distinct regions of the Purkinje cell (i.e. soma, smooth dendrites and spiny dendrites). There is evidence that the soma membrane differs from the dendritic membrane,[15,40,41] but the question of the possible non-uniformity of the dendritic membrane passive resistivity has been more difficult to address. We have assumed that the dendritic membrane is uniform, with a transmembrane resistivity $r_{m,dend}$ which may differ from the value of the soma membrane resistivity $r_{m,soma}$.

The voltage transient in response to an input current step is also to be calculated and compared with the observed voltage transient, as a check. The experimentally observed final relaxation time constant following an intrasomatic hyperpolarizing current step is $\tau_0 = 22 \pm 5$ ms (from Figs 3A, 6C and 9D of Ref. 57), with a similar value observed for intradendritic stimulation.[58] The observed voltage transient is not a simple exponential relaxation; it varies much faster initially than $\exp(-t/\tau_0)$. Peeling[14,74,98] records of voltage transients (Ref. 57 and R. Llinás and M. Sugimori, unpublished) shows that about 0.5 of the total amplitude of a voltage step is contributed by fast transients with time constants of about 3 and 0.5 ms (with the fastest component having an amplitude about seven times larger than that of the slower component). The accuracy of these experimental estimates is limited by the low time resolution of the records at short times and by slow active processes (e.g. causing voltage sag) at long times.

The final electrophysiological observations are to do with the attenuation of long and short voltage pulses as they propagate from the soma into the dendrites. The voltage attenuation of a long pulse has been observed for a Purkinje cell (in guinea-pig cerebellar slice) which was simultaneously impaled by a pair of microelectrodes (R. Llinás and M. Sugimori, unpublished). A rectangular current pulse of 1.5 nA (duration 60 ms) injected at the soma was observed to produce a voltage step of 15.0 mV at the soma and 10.7 mV at the mid-dendritic recording site. Thus, the steady-state voltage attenuation factor ($\Delta V_S/\Delta V_D$), for this double-impaled neuron with $G_{in,soma} = 100.0$ nS, is 1.38 between soma and middle dendrites. In contrast, soma action potentials (duration 0.6 ms full width at half maximum amplitude, Fig. 1C of Ref. 57) are attenuated by a factor of about 7.5 as observed at a mid-dendritic location (Fig. 4 of Ref. 58 and R. Llinás and M. Sugimori, unpublished). The voltage attenuation factors for our model will be calculated and compared with these observed values.

RESULTS

Static calculations

The results of the first set of calculations are those values of the dendritic membrane resistivity ($r_{m,dend}$) and somatic membrane resistivity ($r_{m,soma}$) which are compatible with the experimentally measured value of the input conductance at the soma ($G_{in,soma} = 69.2$ nS). For each choice of soma membrane resistivity and cytoplasm resistivity (r_i), the value of $r_{m,dend}$ was varied until the calculated value of $G_{in,soma}$ agreed with the measured value. In Fig. 5 we have plotted $r_{m,dend}$ as a function of $r_{m,soma}$ and r_i (each of the curves in Figs 5, 7, 8 and 9 was obtained using at least six evenly spaced points). The systems

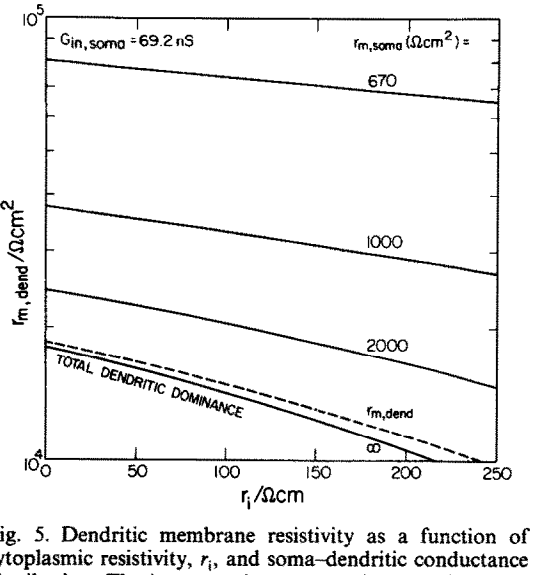

Fig. 5. Dendritic membrane resistivity as a function of cytoplasmic resistivity, r_i, and soma–dendritic conductance distribution. The input conductance at the soma has been held fixed, so $r_{m,dend}$ and $r_{m,soma}$ are inversely related, as are r_m and r_i. Systems with uniform membrane resistivity fall along the dashed curve. The estimated value of $r_{m,dend}$ is much more sensitive to the soma–dendritic conductance distribution than to the cytoplasmic resistivity. Further details in the text.

Table 2. Comparison of final exponential decay time constant (measured at the soma) with average membrane time constant, for several soma–dendritic conductance distributions

$r_{m,soma}$ (Ωcm^2)	$r_{m,dend}$ (Ωcm^2)	ρ* (−)	ρ† (−)	τ_0 (ms)	$\tau_{m,av}$ (ms)
517	∞	0.00	0.00	20.68	17.10
670	74,110	0.29	0.26	18.95	16.89
1000	33,176	0.92	0.79	17.13	16.23
2000	20,403	2.85	2.17	15.40	15.17
14,880	14,880	27.61	8.41	14.00	14.00
∞	14,245	∞	12.57	13.79	13.79

$r_i = 100\,\Omega cm$, $c_{mt} = 1.0\,\mu F/cm^2$, $G_{in,soma} = 69.2$ nS, $G_{leak,soma} = 5.1$ nS.

*Dendritic dominance ratio for the neuron not including the impalement leak, as defined by Rall.[72,74]

†Dendritic dominance ratio with the impalement leak included as part of the total soma conductance.

where the soma conductance is zero are represented by the bottom curve of Fig. 5, labelled "total dendritic dominance", which is also the locus of the smallest values of $r_{m,dend}$ compatible with the measured input conductance of the cell. Systems with uniform soma–dendritic membrane resistivity fall near the limit of total dendritic dominance and have a membrane resistivity of about $15\,k\Omega cm^2$. As the soma conductance increases ($r_{m,soma}$ decreases), less of the total cell conductance is contributed by the dendrites. For $r_{m,soma} = 517\,\Omega cm^2$, the sum of the soma conductance and impalement leak conductance is equal to $G_{in,soma}$ ("total somatic dominance"). The value of $r_{m,dend}$ increases without bound as $r_{m,soma} = 517\,\Omega cm^2$ is approached. The labels "total dendritic dominance" and "total somatic dominance" refer to the unperturbed neuron; the impalement leak on the soma will bias the degree of dendritic dominance of the impaled neuron in the direction of somatic dominance, as may be seen in Table 2.

The next set of calculations evaluates the input conductance at the dendrites ($G_{in,dend}$) for the same model systems as were used to calculate the results in Fig. 5. Since the calculated input conductance for dendritic impalement sites varies from site to site, we have selected 20 dendritic positions at random (as shown in Fig. 6) and have calculated $G_{in,dend}$ as the average over these 20 sites. The spread of the dendritic input conductances is about ± 10 nS for a typical choice of parameter values r_m and r_i. The ratio $G_{in,soma}/G_{in,dend}$ is plotted in Fig. 7 as a function of $r_{m,soma}$ and r_i. In the limit $r_i \to 0$, the cell becomes isopotential and all the curves in Fig. 7 must converge to a single point. As the cytoplasm resistivity increases or as the transmembrane conductance becomes localized on the soma, the difference between the input conductances measured at the soma and dendrites increases, causing the curves in Fig. 7 to diverge. Only the wedge-shaped region between the total somatic dominance and the total dendritic

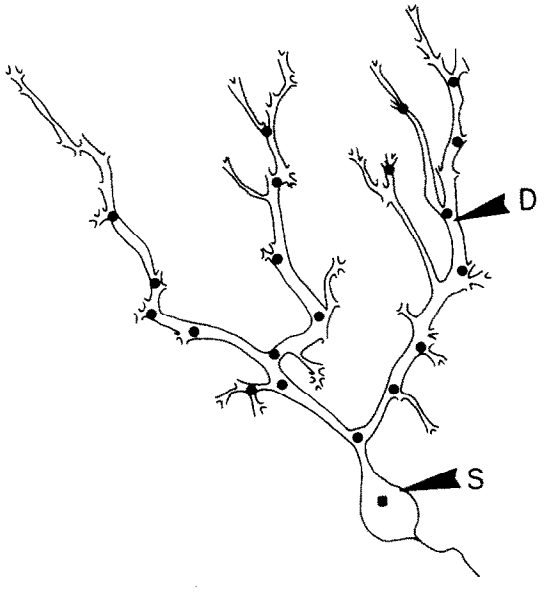

Fig. 6. The 20 dendritic positions at which the dendritic input conductance is evaluated are indicated by the dots. The square marks the somatic impalement site. The dendritic impalement sites were chosen at random by laying a coarse grid over the drawing and marking the places where grid intersections fell on the smooth dendrites (mimicking blind impalement by a microelectrode). Also shown are the sites, marked S and D, which most closely approximate the locations of the microelectrodes for the double-impaled neuron (R. Llinás and M. Sugimori, unpublished) from which pulse attenuation measurements were taken.

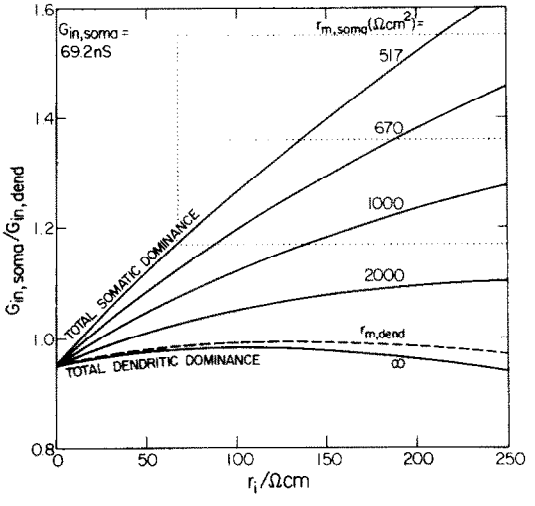

Fig. 7. The ratio of somatic and dendritic input conductances as a function of cytoplasmic resistivity, r_i, and soma–dendritic conductance distribution. The input conductance at the soma has been held fixed. The curves converge to a value smaller than 1.0 as r_i goes to zero because the microelectrode leak at dendritic impalement sites is slightly larger than the leak at the somatic impalement site. Systems with uniform membrane resistivity fall along the dashed curve. The dotted rectangle marks the lower bound of r_i ($=67\,\Omega cm$) and the average and uncertainty of the experimental estimate of $G_{in,soma}/G_{in,dend}$ ($=1.36 \pm 0.19$) for the Purkinje cell. The model best agrees with experiment when its membrane conductance is concentrated on the soma and the cytoplasmic resistivity is greater than $150\,\Omega cm$ (upper-right corner of the diagram).

dominance curves of Fig. 7 is accessible to the model systems satisfying $G_{in,soma} = 69.2$ nS. Systems with uniform soma–dendritic membrane fall close to the lower boundary of the accessible region, where the input conductances at the soma and dendrites are nearly equal. Near the upper boundary of the accessible region, where $r_{m,soma} \rightarrow 517\ \Omega cm^2$ and $r_{m,dend} \rightarrow \infty \Omega cm^2$, one finds that the curves for systems with $r_{m,dend} \geqslant 10^6\ \Omega cm^2$ will differ very little from the curve in Fig. 7 for the limiting case of total somatic dominance. This indicates that the largest value of $r_{m,dend}$ which may be reliably estimated using our model is about $10^6\ \Omega cm^2$. For $r_i = 100\ \Omega cm$, even in the total somatic dominance limit, the model barely agrees with the measured input conductance ratio to within its experimental uncertainty. In order to obtain the observed ratio, values of $r_i > 140\ \Omega cm$ are required. The rough estimate of $r_i \approx 250\ \Omega cm$ made from considerations of bridge balance and extracellular resistivity (see experimental procedures) seems more consistent with the input conductance ratio measurements than does our originally assumed value of $100\ \Omega cm$. However, for either choice of r_i, soma-dominant models are favored.

The next calculation evaluates the steady-state voltage attenuation, $\Delta V_S/\Delta V_D$, between the soma and a mid-dendritic location on the Purkinje cell model when current is injected at the soma. The two recording sites (marked S and D in Fig. 6) were chosen to match as closely as possible the sites used in the actual experiment (R. Llinás and M. Sugimori, unpublished). Impalement leaks of 5.1 and 8.6 nS for the soma and dendritic microelectrodes, respectively, were included. At each value of r_i the values of $r_{m,dend}$ and $r_{m,soma}$ were found such that the model gave $G_{in,soma} = 100.0$ nS and $\Delta V_S/\Delta V_D = 1.38$, as observed. The variation of $r_{m,soma}$ as a function of r_i for these systems is shown in Fig. 8 by the curve labelled "attenuation correct". One may obtain an estimate of r_i by combining the information on voltage attenuation with that for the input conductance ratio. Thus, for each value of r_i we solved for $r_{m,dend}$ and $r_{m,soma}$ such that $G_{in,soma} = 100.0$ nS (with both impalement leaks in place) and $(G_{in,soma}/G_{in,dend})_{bare} = 1.52$ (averaged over the usual 20 dendritic positions shown in Fig. 6 but with the impalement leaks set to zero). The "bare" conductance ratio was used since it eliminated the difference between the double-impaled neuron and the single-impaled neurons for which the conductance ratio was actually measured. The variation of $r_{m,soma}$ as a function of r_i for this calculation is shown in Fig. 8 by the curve labelled "conductance ratio correct". The intersection point of the two curves in Fig. 8 defines the double-impaled neuron model which fits both the observed attenuation factor and conductance ratio; the value of $r_i = 225\ \Omega cm$ at which this occurs provides an estimate of the cytoplasmic resistivity. Since the curves cross at a large angle, this estimate of r_i is relatively insensitive to errors in the experimental measurements (the alternative constraint for the "conductance ratio correct" curve, $G_{in,soma}/G_{m,dend} = 1.36$ with a single impalement leak, would change the estimate of r_i to $220\ \Omega cm$).

Given the above value of r_i, one may immediately determine the parameters for a model which best fits the steady-state data for the average neuron ($G_{in,soma} = 69.2$ nS and $G_{in,soma}/G_{in,dend} = 1.36$). The best average neuron model parameters are $r_{m,dend} = 45{,}740\ \Omega cm^2$, $r_{m,soma} = 760\ \Omega cm^2$ and $r_i = 225\ \Omega cm$. The values of r_m for which the model is compatible with the experimental measurements, to within the experimental uncertainties, covers a range extending a factor of two above and below the average values; this probably reflects the real variability of the population of neurons being sampled. Other static properties for the best average model are the steady-state voltage attenuation, $\Delta V_S/\Delta V_D = 1.23$ (with a pair of leaky microelectrodes included), and the "bare" dendritic dominance ratio, $\rho = 0.50$ (when the soma impalement leak is included, $\rho = 0.44$). The steady-state attenuation factor and input conductance ratio are both sensitive to the value of $r_{m,dend}$. However, the calculated input conductance, conduc-

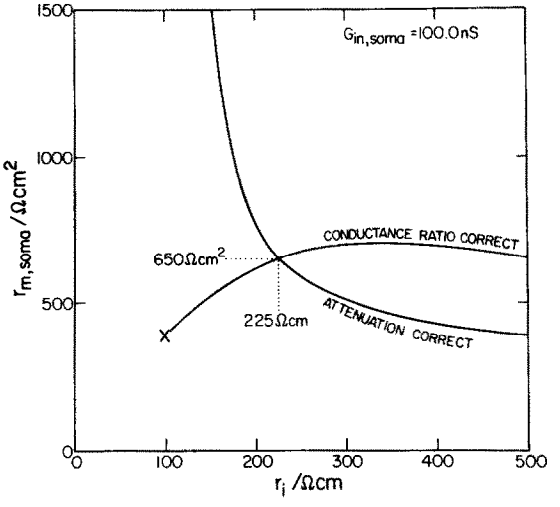

Fig. 8. The two curves show $r_{m,soma}$ as a function of r_i for the double-impaled neuron models which satisfy one or another pair of three possible constraints. In both cases $G_{in,soma}$ was held constant at 100.0 nS (this includes the impalement leaks at sites S and D of Fig. 6), while the soma–dendritic conductance distribution and r_i were allowed to vary. In the case marked "conductance ratio correct" it was also required that $(G_{in,soma}/G_{m,dend})_{bare} = 1.52$ when, for this calculation only, the impalement leaks were set to zero. Solutions were not possible for $r_i < 100\ \Omega cm$. In the case marked "attenuation correct" the second constraint was that the steady-state attenuation of a voltage step applied at S and observed at D was $\Delta V_S/\Delta V_D = 1.38$. Solutions were not possible for $r_i < 120\ \Omega cm$. As one moves along the "conductance ratio correct" curve $r_{m,dend}$ decreases from 40 k Ωcm^2 at $r_i = 150\ \Omega cm$ to $r_{m,dend} = 7.2$ k Ωcm^2 at $r_i = 500\ \Omega cm$, while for the "attenuation correct" curve $r_{m,dend}$ increases from 12 to 120 k Ωcm^2 over the same range of r_i. The point where the two curves cross marks the system which satisfies all three constraints simultaneously. The model parameters in this case are $r_{m,dend} = 19{,}900\ \Omega cm^2$, $r_{m,soma} = 650\ \Omega cm^2$ and $r_i = 225\ \Omega cm$.

tance ratio and attenuation of the model are all insensitive to the way that the membrane conductance of the dendritic compartment is divided between the smooth and spiny dendrites. Shifting the dendritic membrane conductance of the best average neuron model entirely onto the smooth dendrites ($r_{m,smooth} \approx 7.5\,k\,\Omega cm^2$ and $r_{m,spiny} > 10^6\,\Omega cm^2$, for the smooth and spiny dendrites respectively) leaves the calculated properties of the model essentially unchanged.

Dynamic calculations

One may now ask whether the results of dynamic calculations support the estimates of r_m derived on the basis of the static analysis given above. The dynamic behavior of the passive neuron model was investigated by injecting a 0.5 nA hyperpolarizing current step into the soma of the model and calculating the ensuing time evolution of the transmembrane voltage over the next 20 ms or more. From the soma voltage vs time, one may then obtain the final exponential relaxation time constant at the soma, τ_0. The value of τ_0 is about 20 ms (about the same time constant is calculated for dendritic impalements). The precise value of τ_0 obtained in such a calculation depends on the values of the parameters r_i and r_m. In Fig. 9 are plotted the curves of τ_0 as a function of r_i and $r_{m,soma}$, for the same model systems as used in the static calculations. Just as in Fig. 7, the τ_0 curves converge to a point as $r_i \to 0$, and the accessible region on the plot is a wedge bounded by the soma-dominant and dendrites-dominant curves. The models which best agree with the observed average value of $\tau_0 = 22 \pm 5$ ms are essentially the same as those which satisfy the constraints on the static calculations (Fig. 9). The value of $\tau_0 = 19.0$ ms is obtained for the best static neuron model with $c_m = 1.0\,\mu F/cm^2$. This calculated τ_0 is 1.16 times smaller than the observed value, which may be interpreted as being due to experimental uncertainties, an underestimate of the neuron surface area, or an underestimate of the membrane specific capacitance. In the last case the model may be made to fit the observations by simply setting $c_m = 1.16\,\mu F/cm^2$. In any case, the 16% discrepancy is small enough that the results of the dynamic calculation tend to confirm the accuracy and self-consistency of the model.

The shape of the calculated current-clamp voltage transients is not completely described by a single exponential relaxation, but may be approximated as the sum of several successively faster decaying exponential terms as shown in Fig. 10. For our best average neuron model (Fig. 10) the fast transient terms account for 0.38 of the total amplitude of the voltage step, close to the observed value of about 0.5. The time constants of the fast transient terms are calculated to be 3.25, 0.84 and 0.142 ms as compared to the observed values of about 3 and 0.5 ms. The calculations and observations are seen to be in agreement when it is understood that the poor time resolution of the experimental records will not allow the two fastest calculated components to be distinguished. They will instead be seen as a single component with an average decay time near 0.5 ms. Also in agreement with the observations, the fastest component is calculated to have an amplitude six times larger than that of the next fastest component. Thus, the voltage transient calculated with our best average neuron model (where $r_i = 225\,\Omega cm$) seems to

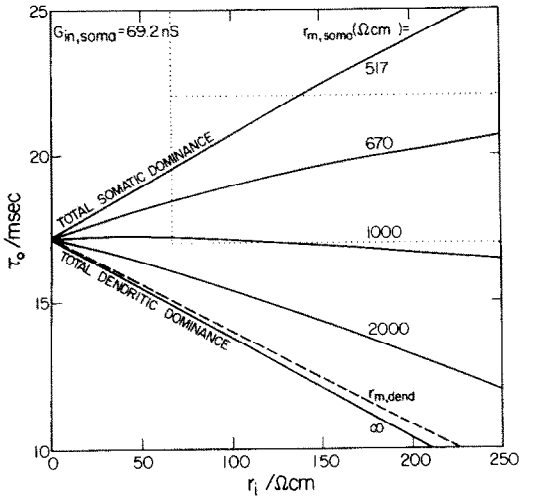

Fig. 9. The final exponential relaxation time constant at the soma as a function of cytoplasmic resistivity, r_i, and soma–dendritic conductance distribution. The input conductance at the soma has been held fixed. Systems with uniform membrane resistivity fall along the dashed curve. The dotted rectangle marks the lower bound of r_i ($= 67\,\Omega cm$) and the average and uncertainty of the experimental estimate of τ_0 ($= 22 \pm 5$ ms) for the Purkinje cell. The model best agrees with experiment when its membrane conductance is concentrated on the soma and the cytoplasmic resistivity is greater than 150 Ωcm (upper-right corner of the diagram).

Fig. 10. Decomposition of a current-clamp voltage transient into a sum of exponential decays. (A) Soma voltage (dots) following a 0.5 nA hyperpolarizing current step applied to the soma. The model parameters are $r_{m,dend} = 45{,}740\,\Omega cm^2$, $r_{m,soma} = 760\,\Omega cm^2$, $r_i = 225\,\Omega cm$, $c_m = 1.0\,\mu F/cm^2$ and $G_{leak,soma} = 5.1$ nS. The applied current drives the soma voltage from the resting value $V(0)$ to a new steady-state value $V(\infty)$. (B) The voltage transient may be approximated as the sum of the four exponential decays shown. (C) On a semilogarithmic plot, it is seen that an exponential decay (straight line) with time constant τ_0 accurately represents the final approach of the soma voltage (dots) to its new steady-state value $V(\infty)$. (D) Subtracting out the final exponential decay reveals a faster decay, with time constant τ_1. (E), (F) Repeating this peeling procedure successively reveals two more exponential decay terms.

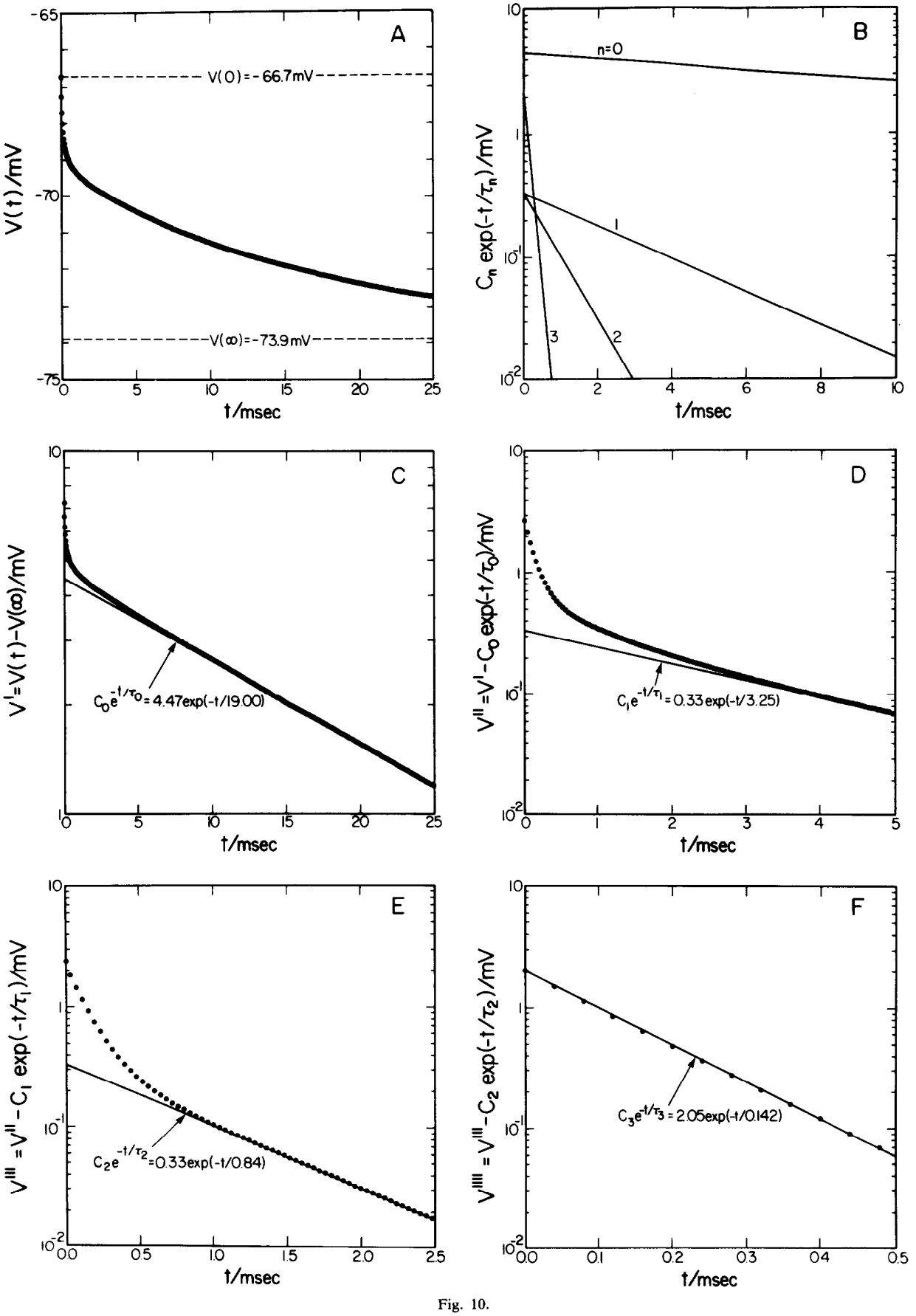
A
V(0)=-66.7mV
V(∞)=-73.9mV
V(t)/mV
t/msec
B
n=0
1
2
3
$C_n \exp(-t/\tau_n)$/mV
t/msec
C
$C_0 e^{-t/\tau_0} = 4.47\exp(-t/19.00)$
$V' = V(t) - V(\infty)$/mV
t/msec
D
$C_1 e^{-t/\tau_1} = 0.33\exp(-t/3.25)$
$V'' = V' - C_0 \exp(-t/\tau_0)$/mV
t/msec
E
$C_2 e^{-t/\tau_2} = 0.33\exp(-t/0.84)$
$V''' = V'' - C_1 \exp(-t/\tau_1)$/mV
t/msec
F
$C_3 e^{-t/\tau_3} = 2.05\exp(-t/0.142)$
$V'''' = V''' - C_2 \exp(-t/\tau_2)$/mV
t/msec

Fig. 10.

Table 3. Comparison of electrotonic lengths, X, for the full model and the equivalent-cylinder approximation, for several soma–dendritic conductance distributions

Description	$r_{m,dend}$ / $r_{m,soma}$ (Ωcm^2)	r_i (Ωcm)	ρ (including leak) (−)	τ_0 / τ_1 / τ_2 / τ_3 (ms)	C_0 / C_1 / C_2 / C_3 (mV)	X_1 / X_2 / X_3 (−)	X_{model} (−)
Dendrites dominant*	14,245	100	12.57	13.79	5.71		
	∞			0.95	0.34	1.074	0.325
				0.085	1.12	0.495	
				—	—	—	
Soma dominant*	∞	100	0.00	20.68	5.88		
	517			1.10	0.30	0.744	0.052
				0.075	1.00	0.379	
				—	—	—	
Best model*	45,740	225	0.44	19.00	4.47		
	760			3.25	0.33	1.427	0.333
				0.84	0.33	1.351	
				0.142	2.05	0.818	
Best model with larger leak†	92,200	233	0.20	21.90	4.52		
	800			3.60	0.31	1.393	0.255
				0.90	0.33	1.301	
				0.142	2.03	0.761	

$X_n = n\pi/\sqrt{(\tau_0/\tau_n) - 1}$ is the equivalent-cylinder electrotonic length.
$c_m = 1.0\,\mu F/cm^2$, $G_{in,soma} = 69.2$ nS.
*$G_{leak,soma} = 5.1$ nS, $V_{rest} = -72$ mV.
†$G_{leak,soma} = 16.8$ nS, $V_{rest} = -88$ mV.

agree well with the shape of the observed transient. Furthermore, as may be seen from Table 3, all the models with $r_i = 100\,\Omega cm$ produce initial transients which are too fast and too small. The initial transients are sensitive to r_i but not to r_m, and the calculated transients are consistent with the observations for $r_i = 225\,\Omega cm$ but not for $r_i = 100\,\Omega cm$.

One may also calculate the response of the model to short current pulses (duration 0.4 ms) applied to the soma to roughly simulate soma action potentials. For the double-impaled neuron model ($r_i = 225\,\Omega cm$, $c_m = 1.0\,\mu F/cm^2$) the resulting soma voltage pulse (0.4 ms full width at half maximum amplitude) is attenuated by a factor of 7.8 in amplitude as observed at the mid-dendritic recording site, in close agreement with the observed attenuation factor of about 7.5. When the calculation is repeated for the best average neuron model the attenuation factor is found to be 7.5, almost unchanged in spite of more than a factor of two increase in $r_{m,dend}$. This indicates that the main load for fast transients is capacitive rather than resistive. Thus, the attentuation of fast transients is determined by c_m and r_i, while the steady-state attenuation is determined by r_m and r_i. Because of the strong attenuation of fast pulses with distance into the dendritic tree, the soma action potential only drives a small fraction of the total cell capacitance, greatly reducing the requiring transmembrane currents at the soma for a given spike amplitude.

Effect of larger electrode leak

Our estimates of V_{rest} and G_{leak} are not independent. So far, we have assumed $V_{rest} = -72$ mV for the unperturbed cell in order to derive the estimates $G_{leak,soma} = 5.1$ nS and $G_{leak,dend} = 8.6$ nS. However, the value of V_{rest} could be much more negative than −72 mV if the leak channel was impermeable to Na^+, and as the assumed value of V_{rest} becomes more negative the estimated size of G_{leak} increases as well. If we assume $V_{rest} = -88$ mV for the unperturbed cell, then our electrode leak estimates increase to $G_{leak,soma} = G_{leak,dend} = 16.8$ nS. In order to assess the effect of a large impalement leak on the parameter estimates derived for our model we have repeated the entire analysis assuming $G_{leak} = 16.8$ nS.

The results of this analysis are given in Table 3 as the "best model with larger leak". The electrical parameters defining this model are $r_{m,dend} = 92.2\,k\,\Omega cm^2$, $r_{m,soma} = 800\,\Omega cm^2$ and $r_i = 233\,\Omega cm$; the value of c_m which makes the model exactly fit the measured time constant $\tau_0 = 22.0$ ms is $c_m = 1.01\,\mu F/cm^2$. Compared with the "best model" in Table 3, one sees that the only significant change in the model is that the estimate of $r_{m,dend}$ doubles when the larger value of G_{leak} is assumed. This indicates that the "best model" parameter estimates, except $r_{m,dend}$, are very stable with respect to perturbations of the model, and that the value of $r_{m,dend}$ for the "best model" is more likely to be an underestimate than an overestimate.

Equivalent-cylinder analysis

Finally, one may ask what the results will be of applying the same sort of equivalent-cylinder analysis to our model as is applied to real neurons.[4,14,40,43,89,95,98] In such an analysis, the neuron is treated as if it were an unbranched membrane cylinder of constant diameter,[41,42,72–75] and the membrane resistivity, r_m, and

the electrotonic length, X, of the cell are obtained from the measurements of successive exponential time constants[74] in a current-clamp experiment. We may find the exponential time constants characterizing our model by applying the "peeling of exponentials" method[74] to the computed voltage vs time for the model, as illustrated in Fig. 10.

In the case of a uniform cable, the final decay time constant, τ_0, is just equal to the membrane time constant, $\tau_m = r_m c_m$.[74] In the equivalent cylinder analysis, one assumes that $\tau_0 = \tau_m$ and obtains the membrane resistivity from the relation $r_m = \tau_0/c_m$. The estimate of r_m so obtained is accurate only when the equality $\tau_0 = \tau_m$ is a good approximation. Since the membrane resistivity of the model neuron is non-uniform, one must generalize the definition of τ_m in order to assess the accuracy of the estimate of r_m obtained through the equivalent cylinder analysis. A suitable generalization for τ_m is given by $\tau_{m,av} = C_{total}/G_{total}$, where C_{total} and G_{total} are the total transmembrane capacitance and conductance of the cell (including the impalement leak). Note that in the case of non-uniform r_m, it is the average membrane conductivity and not the average resistivity that is the relevant quantity. In the limit as $r_i \to 0$, the cell interior becomes isopotential and the final decay time constant is just $\tau_0 = \tau_{m,av}$ for either uniform or non-uniform membrane. For a uniform membrane cylinder with $r_i \neq 0$, one has $\tau_0 = \tau_m = \tau_{m,av}$. The values of τ_0 and $\tau_{m,av}$ for our model are compared in Table 2. For the systems with nearly uniform soma–dendritic membrane (near the bottom of Table 2), $\tau_0 = \tau_{m,av}$ is a good approximation and the estimate $r_m = \tau_0/c_m$ will be accurate (once G_{leak} is accounted for). As the membrane conductance becomes localized on the soma (ascending Table 2), the difference between τ_0 and $\tau_{m,av}$ increases, making the estimate $r_m = \tau_0/c_m$ less reliable. For $r_i = 100\,\Omega$cm the estimated and the actual average membrane conductivities differ by at most 20%, but this difference increases linearly with r_i. Thus, the equivalent cylinder analysis yields only a fair estimate of the average membrane properties when they are spatially very non-uniform.

The second quantity obtained in the equivalent-cylinder analysis is the electrotonic length. For a uniform cable, the voltage transient following a current step may be expressed as $V(t) = V(\infty) + \Sigma_{n=0}^{\infty} C_n \exp(-t/\tau_n)$, where the τ_n are given by a relation in terms of only τ_0 and the electrotonic length X. Inverting this relation one obtains $X = X_n = n\pi/\sqrt{(\tau_0/\tau_n) - 1}$.[74] In Table 3 we compare the equivalent-cylinder electrotonic length estimates, X_n, with the actual electrotonic length of the model, X_{model} (averaged over the three principal dendritic branches). The values X_n are comparable to estimates obtained for real neurons.[4,40,43,95,98] However, even in the case where the membrane resistivity is essentially uniform over the model neuron (dendrites-dominant example), the equivalent-cylinder electrotonic length is substantially different from the actual electrotonic length of the model; the estimate X_1 calculated from the first two decay time constants is in error by a factor of three. In the case of total somatic dominance, where the membrane resistivity is highly non-uniform, the equivalent-cylinder analysis overestimates the electrotonic length by a factor of ten, and for our best model the electrotonic length is overestimated by a factor of four. These erroneously large estimates for the electrotonic length will misleadingly confirm the assumption of spatial uniformity for r_m which is built into the equivalent-cylinder approximation. It appears that the equivalent-cylinder electrotonic length will be very unreliable when the membrane is non-uniform or the branching power differs from 3/2. A symptom of this problem is that the successive estimates X_n are not equal.

DISCUSSION

Main conclusions and internal checks

The first conclusion one may draw from the results of the computer model is that the somatic and dendritic passive membrane resistivities are very different for the Purkinje cell. This conclusion follows directly from the experimentally observed inequality of the dendritic and somatic input conductances, and is very robust in the sense that essentially the same conclusion will be reached in spite of large changes in the electrical and morphological parameters of the model. The electrical parameters determining the input conductance of the model are just r_i and r_m. From Fig. 7 it is clear that the results of the model with uniform membrane resistivity are inconsistent with the observed inequality of the soma–dendritic input conductances, for all values of r_i. To examine the effect of morphological perturbations of the model, consider the effect of changing its overall size. Shrinking the model neuron by 25% causes the ratio $G_{in,soma}/G_{in,dend}$ to increase by 7% for the soma-dominant case but has essentially no effect for the dendrites-dominant case. To significantly alter the conclusion that the cell exhibits soma dominance, the size of the neuron must be misestimated by a factor of two or more; subtle morphological inaccuracies of the model are likely to have an even weaker effect than this. The underlying reason that allows one to derive such a firm conclusion about the spatial distribution of r_m is that the surface area of the dendrites of the Purkinje cell is vastly larger than the surface area of the soma. To obtain the observed ratio of input conductances, the total conductance of the dendrites must be smaller than that of the soma; because of the disproportionately larger dendritic area, this further requires that $r_{m,dend} \gg r_{m,soma}$. The deduction of the non-uniformity of r_m hinges on the availability of both somatic and dendritic input conductance measurements.

The second result of our computer simulations is the quantitative estimation of the values of the pas-

sive membrane resistivities. In order to assess the accuracy of these estimates, we again consider the morphological adequacy of our computer model. First, we argue that it is reasonable to expect that a computer model based on the morphology of a single cell will adequately represent the whole class of Purkinje cells. The Purkinje neurons are relatively homogenous in size and shape over the entire cerebellar cortex and highly stereotyped compared to other neurons.[85] While no two will have precisely the same dendritic arbor, it appears that the differences are random variations on a theme, where each Purkinje cell grows to maximize its synaptic contacts with the uniformly packed parallel fibers which cross its discrete, sheet-like dendritic domain.[7,8,25] The very complexity of the dendritic tree of a single Purkinje cell makes it likely that each cell contains a good sample of all the possible random dendritic subnetworks, and that the detailed differences between individual arbors are averaged out in the evaluation of simple properties such as the input conductance. There is a precedent for our assertion that a single model may accurately represent the morphology and function of a class of neurons, in the case of identified neurons in an invertebrate.[31]

The other aspect of morphological adequacy which bears on our quantitative electrical parameter estimates is the accuracy with which the dimensions of the particular model are determined. Since most of the total passive conductance of this neuron lies on the soma, it follows that the soma membrane conductivity is, except for a factor near unity, just the whole cell conductance divided by the soma area. The smooth, simple shape of the soma[34] means that its size and surface area may be quite accurately determined (though it is not certain that the anatomically defined soma will exactly coincide with the region of enhanced membrane conductivity). We estimate that our determination of the average soma membrane resistivity, $r_{m,soma} = 760\ \Omega cm^2$, has an uncertainty of $\pm 50\%$. The accuracy of $r_{m,dend}$ depends on the accuracy of the membrane surface area estimate for the very complex dendritic tree of the Purkinje cell, but this is probably not the limiting factor (the agreement of calculated and measured values of τ_0 supports an assessment that the error in the dendritic area estimate is of order 20% or less). The accuracy of $r_{m,dend}$ is limited by the experimental uncertainty of the ratio $G_{in,soma}/G_{in,dend}$ from which the dendritic dominance of the model is deduced. On this basis we estimate that the average dendritic membrane resistivity, $r_{m,dend} = 46\ k\Omega cm^2$, has an uncertainty of about a factor of two. However, this estimate ignores the possible non-uniformity of r_m within the dendritic compartment itself. Since the conductance density of the fully activated coupled Ca^{2+}–K^+ channel system is found to be quite large, about $20\ mS/cm^2$ ("r_m" $= 50\ \Omega cm^2$) in another preparation,[52] and since the active conductances on the smooth dendrites may be partially activated even at rest (Fig. 3E of Ref. 58), it is quite plausible that an active conductance contribution makes $r_{m,smooth} \ll r_{m,spiny}$. And since modifying the parameters of the best average model to $r_{m,smooth} \approx 7.5\ k\Omega cm^2$ and $r_{m,spiny} > 10^6\ \Omega cm^2$ would leave the model compatible with all the observations, it is possible that the value $r_{m,dend} = 46\ k\Omega m^2$ underestimates the true passive membrane resistivity by one or more orders of magnitude.

The accuracy of our estimate of r_i depends on the accuracy of the measured lengths and diameters of the smooth dendritic segments, but since the smooth dendrites are quite stout, the measurements of their dimensions should be relatively accurate. An error in r_i proportional to tissue shrinkage is possible, but shrinkage should be accounted for in the construction of our model. We estimate that our value of $r_i = 225\ \Omega cm$ is reliable to $\pm 20\%$. Our deduction of a value for r_i hinges on the availability of somatic and dendritic input conductance and pulse attenuation measurements.

Active conductances

The above discussion assumes that a passive model for the Purkinje cell near rest is essentially correct. However, the presence of active conductances on the dendrites[57,58] calls this assumption into question. There are two aspects to consider. Firstly, one may ask whether the membrane conductances are essentially constant during small hyperpolarizing voltage steps, so that a linear analysis is adequate. The observed linearity of the current–voltage relation in the hyperpolarizing direction, for both soma and dendrites, supports the adequacy of the passive model. The second aspect has to do with whether the estimated membrane resistivities represent truly passive channels or whether they represent the near linear behaviour of a collection of voltage-sensitive channels over a restricted voltage range. In this regard, one observes that the response for small voltage displacements from rest is essentially unchanged by pharmacological block of the Na^+ and Ca^{2+} active conductances.[57,58] This supports the notion that truly passive conductances dominate the electrical behaviour of the Purkinje cell for membrane potentials at or below $-60\ mV$. Also, the effect of the microelectrode leak will tend to linearize the response of the neuron,[41] and this coupled with the relatively small value of the dendritic membrane conductivity will make our estimates of $r_{m,soma}$, r_i and c_m very insensitive to a possible active contribution to $r_{m,dend}$. For exactly the same reason the uncertainty in the value of $r_{m,dend}$ is large. For a more rigorous assessment of the possible active contributions to $r_{m,dend}$ a model incorporating dendritic active conductances is probably necessary.

Supporting evidence

Estimates of r_m which have been made for other mammalian neurons typically fall in the range $1–20\ k\Omega cm^2$,[4,14,20,43,81,83,89,95,98] which is somewhat lower

than our estimate of $r_{m,dend}$ for the guinea-pig Purkinje cell. However, these estimates of r_m have been obtained under the assumption of uniform membrane resistivity, and accordingly they should be compared with the membrane resistivity of 17 kΩcm^2 for our best model suitably averaged over the entire cell. As we have seen from the application of the equivalent-cylinder analysis to our model, electrophysiological measurements at the soma alone will give little or no indication of the spatial non-uniformity of the membrane resistivity, even when the non-uniformity is extreme. Furthermore, the fast components of the membrane voltage transients, upon which estimates of the electrotonic length are based, are subject to systematic errors in the usual single microelectrode–balanced bridge recording arrangement.[27,81,89] Thus, the present results are not incompatible with the work of other authors. Neither is our high estimate of $r_{m,dend}$ without precedent, since the measured soma membrane resistivity for bovine chromaffin cells is 50 kΩcm^2,[28a] while that for *Aplysia* neurons is $r_m = 550$ kΩcm^2.[32] The magnitude of the intrinsic resistivity of artificial bilayer membranes, in the range 10^7–10^8 Ωcm^2,[47,63,88,91] forms a strict upper bound on r_m which is easily compatible with our estimate of $r_{m,dend}$.

Finally, our estimate of $r_{m,soma}$ is confirmed by evidence derived from the measurements of K^+ efflux from guinea-pig Purkinje cell somata.[38] Having assumed $r_m = 2500$ Ωcm^2 for the soma, the increase in the K^+ concentration in the extracellular space around the soma of a Purkinje cell during a dendritic spike was calculated to be 0.06 mM, whereas the observed increase was much larger, near 0.3 mM (see p. 385 and Fig. 4 of Ref. 38). The transmembrane K^+ conductance which is necessary to account for the observed K^+ concentration change at the soma is thus five times larger than that originally assumed in the calculation. During the dendritic spike the soma membrane was depolarized by about 30 mV from rest, to near −35 mV. This is only 5 mV above the threshold for firing somatic spikes (before they are blocked by the prolonged depolarization due to the dendritic spike), so the fast somatic K^+ channel will be near or below threshold.[3] Assuming that the entire transmembrane K^+ efflux of the soma during the dendritic spike is due to the passive membrane conductivity, one obtains $r_{m,soma} = 500$ Ωcm^2, in good agreement with our estimate of 760 Ωcm^2 ± 50%.

Significance of findings

The conclusion that $r_{m,dend} \approx 50$ kΩcm^2 for the Purkinje cell dendrites (with the true passive resistivity possibly much higher) has significant implications for neuronal integration if it may be extended to other neuron types. Consider the motoneuron, where the distal dendritic processes are very long (500 μm) and thin (0.5 μm).[4,96,97] Given the values $r_m = 2500$ Ωcm^2 and $r_i = 70$ Ωcm which have been estimated for the motoneuron,[4] the electrotonic length of such a dendritic cable is about 2.4. This is so long that a synaptic current injected near the terminal end of the cable will be dissipated as it propagates down the cable. Seen from the soma, these fine terminal processes will appear to be useless since passive spread of signals from the terminal processes to the soma is ineffective. However, if the membrane resistivity of this dendritic cable is 50 kΩcm^2 instead, then its electrotonic length falls from 2.4 to 0.5 and the situation becomes very different. The dendritic cable is now so electronically short that even synaptic currents injected at the terminal end of the dendrite will travel the length of the cable with little dissipation; because of the distributed capacitance of the cable, a current pulse onto the cable will have its amplitude reduced and its duration correspondingly increased as it travels along the cable.[5,40,42,77] Seen from the soma, distal and proximal synapses on the dendrite will appear equally effective, though in different roles. The short, high amplitude pulses from proximal synapses will be most effective in eliciting immediate action potentials, while the longer, lower amplitude pulses from distal synapses will be most effective in integrating temporally asynchronous inputs. We have framed an extreme example here, but the argument applies to a wide range of neuron types (e.g. motoneurons, pyramidal cells, stellate cells[36]) which have fine, long terminal dendritic processes.

The non-uniformity of the "passive" membrane resistivity is highly plausible in the light of functional considerations. The high value of $r_{m,dend}$ may be readily understood as a specialization which optimizes the dendrites for signalling with minimum attenuation. The low value of $r_{m,soma}$ may be viewed instead as a specialization to maintain stability of the soma membrane voltage in the face of the large high-threshold fast Na^+ and low-threshold slow Na^+ conductances.[57] These voltage-dependent Na^+ channels provide positive feedback to membrane voltage fluctuations and have the potential for explosive instability. This instability is used to good effect to generate the action potential but must be controlled by a large, hyperpolarizing background conductance.

There is evidence that the resting potential is actually set by a specific mixed Na^+–K^+ conductance channel which behaves as if it were a passive leakage conductance near V_{rest}.[21,61] If this is so, then it may be that the intrinsic membrane leakage conductivity is relatively constant over the cell and close to the intrinsic leakage conductivity of a pure lipid bilayer. Any conductivity above this very small intrinsic conductivity would then be due to specific ion channels "deliberately" inserted into the membrane. The spatial non-uniformity of r_m would be merely a consequence of the well-documented non-uniform distribution of specific ion channels on neurons,[57–59] and not an intrinsic property of the membrane at all.

So far we have considered the significance of the large value of the dendritic membrane resistivity

deduced with our model in the context of a neuron with synaptic inputs sparsely distributed over its surface. But the firing rates of the neurons, axons and synapses in the cerebellar cortex is of order 50 Hz.[26,62,90] Consider a portion of spiny dendrite 1.0 μm in diameter, with a synaptic density of 4.4 synapses/μm (on spines) and with each synapse firing at an average rate of 10 Hz. If we take the integrated conductance of each synaptic pulse to be 4.0 nS ms,[5] and ignore for the moment the effect of the spine stem, then the effect of the synapses is to produce an average transmembrane conductance density of 5.6 mS/cm^2 ("r_m" = 180 Ωcm^2) for this dendrite. In the case of dense synaptic input, with r_m as large as 50 kΩcm^2, the properties of the dendritic cable will be determined by its average synaptic input and the passive membrane conductivity of 0.02 mS/cm^2 will be only a negligibly small perturbation. Similarly, for the smooth dendrites one may expect active conductance densities of a few mS/cm^2 for the coupled Ca^{2+}–K^+ system (at a transmembrane voltage of about −40 mV[52] as in a functioning Purkinje cell[57,58]), again swamping the passive membrane conductivity. The Purkinje cell dendrites are able to generate spikes under some circumstances, by means of a slow Ca^{2+} active conductance.[53,54,58] Dendritic spikes and active graded responses may act as a booster mechanism[53,98] to overcome the electrotonic lengthening of the dendrites due to synaptic activation. The coupled Ca^{2+}–K^+ dendritic conductances may also serve more subtle integrative and regulatory functions such as have been observed elsewhere mediated by the calcium ion.[44,46,52,53,78] Clearly, the passive leakage conductance of the dendrites is ignorable in comparison with the tonic synaptic and active conductances present on a functioning Purkinje cell.

The large value of the cytoplasmic resistivity deduced with our model has significant consequences. For r_i = 225 Ωcm the resistance of the stem of a spine (0.7 μm long and 0.14 μm diameter) will be about 100 MΩ, as compared with the peak conductance of about 15 nS (67 MΩ)[5] for an activated synapse. Thus, the conductance pulse for a synapse-on-spine will be only about half as large as for the synapse directly on a dendrite. This may be important in preventing dense synaptic input from overloading a dendritic cable and also in possibly providing a postsynaptic means for modulating synaptic conductances. The other aspect of a large r_i is that it provides the various neuronal compartments with some electrical autonomy. It is metabolically cheaper to produce electrotonic isolation by increasing r_i rather than by decreasing r_m, and the isolation so obtained may be overridden by means of active responses (e.g. a dendritic spike) when required. Such flexibility may be desirable for central neurons in order to allow both local processing of information as well as integration of inputs at the soma.

Acknowledgement—The author wishes to thank Dr. R. Llinás for providing his unpublished data.

REFERENCES

1. Adams P. R. and Brown D. A. (1975) Actions of γ-aminobutyric acid on sympathetic ganglion cells. *J. Physiol., Lond.* **250,** 85–120.
2. Angaut P., Alvarado-Mallart R. M. and Sotelo C. (1982) Ultrastructural evidence for compensatory sprouting of climbing and mossy afferents to the cerebellar hemisphere after ipsilateral pedunculotomy in the newborn rat. *J. comp. Neurol.* **205,** 101–111.
3. Barrett E. F., Barrett J. N. and Crill W. E. (1980) Voltage-sensitive outward currents in cat motoneurones. *J. Physiol., Lond.* **304,** 251–276.
4. Barrett J. N. and Crill W. E. (1974) Specific membrane properties of cat motoneurones. *J. Physiol., Lond.* **239,** 301–324.
5. Barrett J. N. and Crill W. E. (1974) Influence of dendritic location and membrane properties on the effectiveness of synapses on cat motoneurones. *J. Physiol., Lond.* **239,** 325–345.
6. Berry M. and Bradley P. (1976) The growth of the dendritic trees of Purkinje cells in the cerebellum of the rat. *Brain Res.* **112,** 1–35.
7. Berry M. and Bradley P. (1976) The application of network analysis to the study of branching patterns of large dendritic fields. *Brain Res.* **109,** 111–132.
8. Berry M., McConnell P. and Sievers J. (1980) Dendritic growth and the control of neuronal form. In *Current Topics in Developmental Biology* (eds Moscona A. A. and Monroy A.). Vol. 15, pp. 67–101. Academic Press, New York.
9. Bishop G. A. (1982) The pattern of distribution of the local axonal collaterals of Purkinje cells in the intermediate cortex of the anterior lobe and paramedian lobule of the cat cerebellum. *J. comp. Neurol.* **210,** 1–9.
10. Bishop G. A., McCrea R. A., Lighthall J. W. and Kitai S. T. (1979) An HRP and autoradiographic study of the projection from the cerebellar cortex to the nucleus interpositus anterior and nucleus interpositus posterior of the cat. *J. comp. Neurol.* **185,** 735–756.
11. Bower J. M. and Woolston D. C. (1983) Congruence of spatial organization of tactile projections to granule cell and Purkinje cell layers of cerebellar hemispheres of the albino rat: vertical organization of cerebellar cortex. *J. Neurophysiol.* **49,** 745–766.
12. Bradley P. and Berry M. (1976) Quantitative effects of climbing fibre deafferentation on the adult Purkinje cell dendritic tree. *Brain Res.* **112,** 133–140.
13. Brown K. T. and Flaming D. G. (1977) New microelectrode techniques for intracellular work in small cells. *Neuroscience* **2,** 813–827.
14. Brown T. H., Fricke R. A. and Perkel D. H. (1981) Passive electrical constants in three classes of hippocampal neurons. *J. Neurophysiol.* **46,** 812–827.

15. Carpenter D. O. (1977) Membrane excitability. In *Mammalian Cell Membranes* (eds Jamieson G. A. and Robinson D. M.). Vol. 4, pp. 184–206. Butterworths, London.
16. Carpenter D. O., Hovey M. M. and Bak A. F. (1971) Intracellular conductance of *Aplysia* neurons and squid axon as determined by a new technique. *Int. J. Neurosci.* **2,** 35–48.
17. Carpenter D. O., Hovey M. M. and Bak A. F. (1973) Measurement of intracellular conductivity in *Aplysia* neurons: evidence for organization of water and ions. *Ann. N.Y. Acad. Sci.* **204,** 502–533.
18. Chowdhury T. K. (1969) Fabrication of extremely fine glass micropipette electrodes. *J. scient. Instrum.* **2,** 1087–1090.
19. Cole K. S. (1972) *Membranes, Ions and Impulses.* University of California Press, Berkeley.
20. Connors B. W., Gutnick M. J. and Prince D. A. (1982) Electrophysiological properties of neocortical neurons *in vitro*. *J. Neurophysiol.* **48,** 1302–1320.
21. Constanti A. and Galvan M. (1983) Fast inward-rectifying current accounts for anomalous rectification in olfactory cortex neurones. *J. Physiol., Lond.* **335,** 153–178.
22. Crepel F. and Delhaye-Bouchaud N. (1978) Intracellular analyses of synaptic potentials in cerebellar Purkinje cells of the rat. *Brain Res.* **155,** 176–181.
23. Crepel F., Dhanjal S. S. and Garthwaite J. (1981) Morphological and electrophysiological characteristics of rat cerebellar slices maintained *in vitro*. *J. Physiol., Lond.* **316,** 127–138.
24. Dahlquist G. and Björk A. (1974) *Numerical Methods*, Chap. 8, Prentice-Hall, Englewood Cliffs, New Jersey.
25. Eccles J. C. (1977) An instruction-selection theory of learning in the cerebellar cortex. *Brain Res.* **127,** 327–352.
26. Eccles J. C., Ito M. and Szentágothai J. (1967) *The Cerebellum as a Neuronal Machine.* Springer, Berlin.
27. Engel E., Barcilon V. and Eisenberg R. S. (1972) The interpretation of current–voltage relations recorded from a spherical cell with a single microelectrode. *Biophys. J.* **12,** 384–403.
28. Farkas D. L., Korenstein R. and Malkin S. (1984) Electroluminescence and the electrical properties of the photosynthetic membrane I. Initial kinetics and the charging capacitance of the membrane. *Biophys. J.* **45,** 363–373.
28a. Fenwick E. M., Marty A. and Neher E. (1982) A patch-clamp study of bovine chromaffin cells and their sensitivity to acetylcholine. *J. Physiol., Lond.* **331,** 577–597.
29. Franck G. (1972) Brain slices. In *The Structure and Function of Nervous Tissue* (ed. Bourne G. H.). Vol. 6, pp. 417–465. Academic Press, New York.
30. Gear C. W. (1971) *Numerical Initial Value Problems in Ordinary Differential Equations*, Chap. 11. Prentice-Hall, Englewood Cliffs, New Jersey.
31. Glantz R. M. and Viancour T. (1983) Integrative properties of crayfish medial giant neuron: steady-state model. *J. Neurophysiol.* **50,** 1122–1142.
32. Graubard K. and Calvin W. H. (1979) Presynaptic dendrites: implications of spikeless synaptic transmission and dendritic geometry. In *The Neurosciences, Fourth Study Program* (eds Schmitt F. O. and Worden F. G.), pp. 317–331. MIT Press, Cambridge, Massachusetts.
33. Hamill O. P., Marty A., Neher E., Sakmann B. and Sigworth F. J. (1981) Improved patch-clamp techniques for high-resolution current recording from cells and cell-free membrane patches. *Pflügers Arch. ges. Physiol.* **391,** 85–100.
34. Hámori J. and Szentágothai J. (1965) The Purkinje cell baskets: ultrastructure of an inhibitory synapse. *Acta biol. hung.* **15,** 465–479.
35. Harvey J. A., Scholfield C. N. and Brown D. A. (1974) Evoked surface-positive potentials in isolated mammalian olfactory cortex. *Brain Res.* **76,** 235–245.
36. Hillman D. E. (1979) Neuronal shape parameters and substructures as a basis of neuronal form. In *The Neurosciences, Fourth Study Program* (eds Schmitt F. O. and Worden F. G.), pp. 477–498. MIT Press, Cambridge, Massachusetts.
37. Hollingworth T. and Berry M. (1975) Network analysis of dendritic fields of pyramidal cells in neocortex and Purkinje cells in the cerebellum of the rat. *Phil. Trans. R. Soc. Ser. B* **270,** 227–264.
38. Hounsgaard J. and Nicholson C. (1983) Potassium accumulation around individual Purkinje cells in cerebellar slices from the guinea-pig. *J. Physiol., Lond.* **340,** 359–388.
39. Hounsgaard J. and Yamamoto C. (1979) Dendritic spikes in Purkinje cells of the guinea-pig cerebellum studied *in vitro*. *Expl Brain Res.* **37,** 387–398.
40. Iansek R. and Redman S. J. (1973) An analysis of the cable properties of spinal motoneurones using a brief intracellular current pulse. *J. Physiol., Lond.* **234,** 613–636.
41. Jack J. (1979) An introduction to linear cable theory. In *The Neurosciences, Fourth Study Program* (eds Schmitt F. O. and Worden F. G.), pp. 324–437. MIT Press, Cambridge, Massachusetts.
42. Jack J. J., Noble D. and Tsien R. W. (1975) *Electric Current Flow in Excitable Cells.* Clarendon, Oxford.
43. Johnston D. and Brown T. H. (1983) Interpretation of voltage-clamp measurements in hippocampal neurons. *J. Neurophysiol.* **50,** 464–486.
44. Kandel E. R. and Schwartz H. (1982) Molecular biology of learning: modulation of transmitter release. *Science, N.Y.* **218,** 433–443.
45. Koch C., Poggio T. and Torre V. (1983) Non-linear interactions in a dendritic tree: localization, timing and role in information processing. *Proc. natn. Acad. Sci. U.S.A.* **80,** 2799–2802.
46. Kostyuk P. G. (1980) Calcium ionic channels in electrically excitable membrane. *Neuroscience* **5,** 945–959.
47. Kotyk A. and Janacek K. (1970) *Cell Membrane Transport.* Plenum, New York.
48. Landis D. M. D. and Reese T. S. (1974) Differences in membrane structure between excitatory and inhibitory synapses in the cerebellar cortex. *J. comp. Neurol.* **155,** 93–126.
49. Lanthier R. and Schanne O. (1966) Change in microelectrode resistance in solutions of different resistivities. *Naturwissenschaften* **53,** 430.
50. Larramendi L. M. H. and Victor T. (1967) Synapses on the Purkinje cell spines in the mouse: an electronmicroscopic study. *Brain Res.* **5,** 15–30.
51. Lev-Tov A., Miller J. P., Burke R. E. and Rall W. (1983) Factors that control amplitude of EPSPs in dendritic neurons. *J. Neurophysiol.* **50,** 399–412.
52. Lewis R. S. and Hudspeth A. J. (1983) Voltage- and ion-dependent conductances in solitary vertebrate hair cells. *Nature* **304,** 538–541.
53. Llinás R. (1979) The role of calcium in neuronal function. In *The Neurosciences, Fourth Study Program* (eds Schmitt F. O. and Worden F. G.), pp. 555–571. MIT Press, Cambridge, Massachusetts.

54. Llinás R. and Hess R. (1976) Tetrodotoxin-resistant dendritic spikes in avian Purkinje cells. *Proc. natn. Acad. Sci. U.S.A.* **73,** 2520–2523.
55. Llinás R. and Hillman D. E. (1969) Physiological and morphological organization of the cerebellar circuits in various vertebrates. In *Neurobiology of Cerebellar Evolution and Development* (ed. Llinás R.), pp. 43–73. Am. Med. Ass., Chicago.
56. Llinás R. and Nicholson C. (1976) Reversal properties of climbing fiber potential in cat Purkinje cells: an example of a distributed synapse. *J. Neurophysiol.* **39,** 311–323.
57. Llinás R. and Sugimori M. (1980) Electrophysiological properties of *in vitro* Purkinje cell somata in mammalian cerebellar slices. *J. Physiol., Lond.* **305,** 171–195.
58. Llinás R. and Sugimori M. (1980) Electrophysiological properties of *in vitro* Purkinje cell dendrites in mammalian cerebellar slices. *J. Physiol., Lond.* **305,** 197–213.
59. Llinás R. and Yarom Y. (1981) Properties and distribution of ionic conductances generating electroresponsiveness of mammalian inferior olivary neurones *in vitro*. *J. Physiol., Lond.* **315,** 569–584.
60. Martinez F. E., Crill W. E. and Kennedy T. T. (1971) Electrogenesis of the cerebellar Purkinje cell response in cats. *J. Neurophysiol.* **34,** 348–356.
61. Mayer M. L. and Westbrook G. L. (1983) A voltage-clamp analysis of inward (anomalous) rectification in mouse spinal sensory ganglion neurones. *J. Physiol., Lond.* **340,** 19–45.
62. Miles F. A., Fuller J. H., Braitman D. J. and Dow B. M. (1980) Long-term adaptive changes in primate vestibuloocular reflex. III. Electrophysiological observations in flocculus of normal monkeys. *J. Neurophysiol.* **43,** 1437–1476.
63. Mueller P. (1979) The mechanism of electrical excitation in lipid bilayers and cell membranes. In *The Neurosciences, Fourth Study Program* (eds Schmitt F. O. and Worden F. G.), pp. 641–658. MIT Press, Cambridge, Massachusetts.
64. Nicholson C. (1979) Brain-cell microenvironment as a communication channel. In *The Neurosciences, Fourth Study Program* (eds Schmitt F. O. and Worden F. G.), pp. 457–476. MIT Press, Cambridge, Massachusetts.
65. Nicholson C. and Freeman J. A. (1975) Theory of current source-density analysis and determination of conductivity tensor for anuran cerebellum. *J. Neurophysiol.* **38,** 356–368.
66. Nicholson C. and Phillips J. M. (1981) Ion diffusion modified by tortuosity and volume fraction in the extracellular microenvironment of the rat cerebellum. *J. Physiol., Lond.* **321,** 225–257.
67. Palkovits M., Magyar P. and Szentágothai J. (1972) Quantitative histological analysis of the cerebellar cortex in the cat. IV. Mossy fiber–Purkinje cell numerical transfer. *Brain Res.* **45,** 15–29.
68. Pellionisz A. (1979) Modeling of neurons and neuronal networks. In *The Neurosciences, Fourth Study Program* (eds Schmitt F. O. and Worden F. G.), pp. 525–546. MIT Press, Cambridge, Massachusetts.
69. Pellionisz A. and Llinás R. (1977) A computer model of cerebellar Purkinje cells. *Neuroscience* **2,** 37–48.
70. Pethig R. (1979) *Dielectric and Electronic Properties of Biological Materials*, Chap. 7. Wiley, New York.
71. Purves R. D. (1979) The physics of iontophoretic pipettes. *J. Neurosci. Meth.* **1,** 165–178.
72. Rall W. (1959) Branching dendritic trees and motoneuron membrane resistivity. *Expl Neurol.* **1,** 491–527.
73. Rall W. (1962) Theory of physiological properties of dendrites. *Ann. N.Y. Acad. Sci.* **96,** 1071–1092.
74. Rall W. (1969) Time constants and electrotonic lengths of membrane cylinders and neurons. *Biophys. J.* **9,** 1483–1508.
75. Rall W. and Rinzel J. (1973) Branch input resistance and steady attenuation for input to one branch of a dendritic neuron model. *Biophys. J.* **13,** 648–688.
76. Ranck J. B. and BeMent S. L. (1965) The specific impedance of the dorsal columns of cat: an anisotropic medium. *Expl Neurol.* **11,** 451–463.
77. Redman S. J. (1973) The attenuation of passively propagating dendritic potentials in a motoneurone cable model. *J. Physiol., Lond.* **234,** 637–664.
78. Reuter H. (1983) Calcium channel modulation by neurotransmitters, enzymes and drugs. *Nature* **301,** 569–574.
79. Robinson R. A. and Stokes R. H. (1959) *Electrolyte Solutions*. Chap. 6 and Appendix 6. Butterworths, London.
80. Schanne O. F., Lavallée M., Laprade R. and Gagné S. (1968) Electrical properties of glass microelectrodes. *Proc. Inst. electl electron Engr* **56,** 1072–1082.
81. Schanne O. F. and Ruiz P.-Ceretti E. (1978) *Impedance Measurements in Biological Cells*. Wiley, New York.
82. Schmitt F. O., Dev P. and Smith B. H. (1976) Electrotonic processing of information by brain cells. *Science, N.Y.* **193,** 114–120.
83. Scholfield C. N. (1978) Electrical properties of neurones in the olfactory cortex slice *in vitro*. *J. Physiol., Lond.* **275,** 535–546.
84. Segal M. and Barker J. L. (1984) Rat hippocampal neurons in culture: properties of GABA-activated Cl^- ion conductance. *J. Neurophysiol.* **51,** 500–515.
85. Shepherd G. M. (1979) *The Synaptic Organization of the Brain*, Chap. 10. Oxford University Press, New York.
86. Somogyi P. and Hámori J. (1976) A quantitative electron microscopic study of the Purkinje cell axon initial segment. *Neuroscience* **1,** 361–365.
87. Sotelo C. (1976) Morphology of the cerebellar cortex. In *Frog Neurobiology* (eds Llinás R. and Precht W.), pp. 864–891. Springer, Berlin.
88. Strichartz G. R. (1977) The composition and structure of excitable nerve membrane. In *Mammalian Cell Membranes* (eds Jamieson G. A. and Robinson D. M.). Vol. 3, pp. 172–205. Butterworths, London.
89. Sugimori M., Preston R. J. and Kitai S. T. (1978) Response properties and electrical constants of caudate nucleus neurons in the cat. *J. Neurophysiol.* **41,** 1662–1675.
90. Suzuki D. A., Noda H. and Kase M. (1981) Visual and pursuit eye movement-related activity in posterior vermis of monkey cerebellum. *J. Neurophysiol.* **46,** 1120–1139.
91. Ting-Beall H. P., Lees M. B. and Robertson J. D. (1979) Interactions of Foch–Lees proteolipid apoprotein with planar lipid layers. *J. Membr. Biol.* **51,** 33–46.
92. Traub R. D. (1982) Simulation of intrinsic bursting in CA3 hippocampal neurons. *Neuroscience* **7,** 1233–1242.
93. Traub R. D. and Llinás R. (1977) The spatial distribution of ionic conductances in normal and axotomized motoneurons. *Neuroscience* **2,** 829–849.
94. Traub R. D. and Llinás R. (1979) Hippocampal pyramidal cells: significance of dendritic ionic conductances for neuronal function and epileptogenesis. *J. Neurophysiol.* **42,** 476–496.

95. Turner D. A. and Schwartzkroin P. A. (1980) Steady-state electrotonic analysis of intracellularly stained hippocampal neurons. *J. Neurophysiol.* **44,** 184–199.
96. Ulfhake B. and Cullheim S. (1981) A quantitative light microscopic study of the dendrites of cat spinal γ-motoneurons after intracellular staining with horseradish peroxidase. *J. comp. Neurol.* **202,** 585–596.
97. Ulfhake B. and Kellerth J-O. (1981) A quantitative light microscopic study of the dendrites of cat spinal α-motoneurons after intracellular staining with horseradish peroxidase. *J. comp. Neurol.* **202,** 571–583.
98. Vogt B. A. and Gorman A. L. F. (1982) Responses of cortical neurons to stimulation of corpus callosum *in vitro*. *J. Neurophysiol.* **48,** 1257–1273.
99. Yedlin M., Kwan H., Murphy J. T., Ngugen-Huu H. and Wong Y. C. (1974) Electrical conductivity in cat cerebellar cortex. *Expl Neurol.* **43,** 555–569.

(*Accepted* 28 *June* 1984)